Dynamic axonal translation in developing and mature visual circuits

Toshiaki Shigeoka[1,4], Hosung Jung[2,4,5], Jane Jung[2], Benita Turner-Bridger[1], Jiyeon Ohk[2], Julie Qiaojin Lin[1], Paul S. Amieux[3], Christine E. Holt[1,5]

[1]Department of Physiology, Development and Neuroscience, University of Cambridge, Downing Street, Cambridge, CB2 3DY, United Kingdom.

[2]Department of Anatomy, Brain Research Institute, and Brain Korea 21 PLUS Project for Medical Science, Yonsei University College of Medicine, Seoul, 03722, Republic of Korea.

[3]Bastyr University Research Institute, Bastyr University, Kenmore, WA 98028, USA.

[4]Co-first author

[5]Co-senior author

*Correspondence should be addressed to H.J. (hosungjung@yonsei.ac.kr) or C.E.H. (ceh33@cam.ac.uk)

SUMMARY

Local mRNA translation mediates the adaptive responses of axons to extrinsic signals but direct evidence that it occurs in mammalian CNS axons *in vivo* is scant. We developed an axon-TRAP-RiboTag approach in mouse that allows deep-sequencing analysis of ribosome-bound mRNAs in the retinal ganglion cell axons of the developing and adult retinotectal projection *in vivo*. The embryonic-to-postnatal axonal translatome comprises an evolving subset of enriched genes with axon-specific roles suggesting distinct steps in axon wiring, such as elongation, pruning and synaptogenesis. Adult axons, remarkably, have a complex translatome with strong links to axon survival, neurotransmission and neurodegenerative disease. Translationally co-regulated mRNA subsets share common upstream regulators, and sequence elements generated by alternative splicing promote axonal mRNA translation. Our results indicate that intricate regulation of compartment-specific mRNA translation in mammalian CNS axons supports the formation and maintenance of neural circuits *in vivo*.

INTRODUCTION

RNA localization and local translation are evolutionarily conserved mechanisms employed by cells to control the precise subcellular positioning of nascent proteins. Neurons are highly compartmentalized cells with functionally distinct cytoplasmic/membrane domains (dendrites, axons, and somas), and emerging evidence indicates that localized mRNA translation supports this subcellular differentiation (Holt and Schuman, 2013; Martin and Ephrussi, 2009). Recent *in vitro* studies revealed an unexpectedly large population of mRNAs in axons, and inhibiting the translation of just one or two of them can cause specific defects in fundamental axonal behaviors, such as neurotrophin-induced outgrowth, branching, cue-induced chemotropic responses and injury-induced regeneration (references in (Jung et al., 2012)). *In vitro* studies have also provided evidence that extrinsic signals, such as guidance cues and growth factors, selectively induce rapid axonal synthesis of distinct protein subsets (references in (Jung et al., 2012)). A rational interpretation of these results is that specific subsets of mRNAs are coordinately translated when required while most axonally localized mRNAs remain translationally repressed. Thus, to understand the function of axonal mRNA translation, it is important to carry out a comprehensive and unbiased global analysis of the mRNAs that are specifically translated in the axonal compartment *in vivo*.

The axons of retinal ganglion cells (RGCs) terminate in the superior colliculus (SC) of the midbrain. A point-to-point topographic projection of RGC axons to the SC allows the brain to reconstruct a map of the outside world. In mouse, the formation of this retinotopic map in the SC can be divided into three distinct phases (Feldheim and O'Leary, 2010). First, embryonic RGC axons enter the SC and initially extend beyond their topographically correct "termination zones (TZs)" without branching or synapsing (*elongation* period). Second, interstitial branches arise from the primary axon shafts of RGCs in their appropriate TZs and begin to form synapses (*branching*/*synaptogenesis* period). Third, in the first two postnatal weeks, correctly wired axon branches are strengthened and excess inappropriate branches are pruned (*pruning* period) resulting in the mature topographic map in adulthood (Fig. 1A)

(Godement et al., 1984). Intriguingly, evidence suggests that local mRNA translation in the RGC axons may regulate subtle aspects of the formation of the retinotectal projection *in vivo* (Brunet et al., 2005). It is not known, however, which mRNAs are axonally translated and which specific aspects of visual circuit assembly they affect.

To address this issue, we developed axon-TRAP (Translating Ribosome Affinity Purification) in mouse, a method that allows specific isolation of ribosome-bound mRNAs in the distal compartment of RGC axons *in vivo*. Analysis of these axon-specific translatomes at multiple ages reveals that axonal translation may play two major roles: regulation of protein and energy homeostasis, which is supported by mRNAs constitutively translated regardless of developmental stage; and regulation of stage-specific events, such as axon elongation, branching, pruning, synapse formation and synaptic transmission, which is supported by mRNAs whose translation is developmentally regulated. We also found that axonal mRNA translation continues in adulthood, when regulators of neurotransmission and axon survival are locally translated. Bioinformatic analysis of key translational regulators such as mammalian target of rapamycin complex 1 (mTORC1), fragile X mental retardation protein (FMRP) and adenomatous polyposis coli (APC), reveals that their target mRNAs are translationally co-regulated in a stage-specific manner. In addition, axonally translated mRNAs show extensive isoform diversity, yet only one single isoform is usually translated at any given time and these axonally translated isoforms share common regulatory sequence motifs that promote axonal mRNA translation. Collectively, the results provide direct evidence for the occurrence of developmental stage-specific, compartmentalized mRNA translation in developing and mature CNS axons and provide a deeper understanding of the molecular machinery involved in CNS wiring and maintenance.

RESULTS

1. Retinal RiboTag labels RGC axonal ribosomes *in vivo*

In order to isolate mRNAs translating in RGC axon terminals in the SC *in vivo*, we used the RiboTag knock-in mouse line (Sanz et al., 2009), in which Cre-mediated recombination switches the RiboTag allele, which encodes the 60S subunit protein ribosomal protein L22 (rpL22), to the hemagglutinin (HA)-tagged rpL22 allele (HA-rpL22). We crossed this mouse with Pax6-alpha-Cre mouse (Marquardt et al., 2001), which transiently expresses Cre in the neural progenitors in the peripheral retinal primordium, permanently labeling RGCs (Fig. 1B, green area in the eye). We confirmed that no resident cells in the SC express Cre by two independent approaches, histological and molecular biological assay (Figs. 1CD & S1, see Extended Experimental Procedures). Therefore, the immunopurification of ribosome-mRNA complexes from the dissected SC allows us to profile local translation in axon terminals of RGCs *in vivo* (axon-TRAP) (Fig. 1B).

We sought to visualize the labeled ribosomes using an HA antibody. HA-immunoreactivity was observed in the distal neural retina (Figs. 1E and S1) and the optic nerve head (ONH) (Fig. 1E, white box), the soma-free region where RGC axons collect to exit the eye, indicating that the RGC axons do contain HA-tagged ribosomes. To visualize the tagged ribosomes with higher resolution, we employed immuno-electron microscopy (EM). Immuno-gold particles specifically labeled a subpopulation of ultrastructurally identifiable ribosomes (Fig. 1F) in the distal neural retina in a Cre-dependent manner (Fig. 1G). We successfully detected HA-tagged ribosomes in the axon shaft in the ONH and the optic nerve (ON) (Fig. 1HI) and presynaptic terminals in the SC (Fig. 1J-L), indicating that HA-labeled endogenous ribosomes are transported to the axon. Together, our histological, molecular biological, and ultrastructural analyses indicate that Retinal RiboTag faithfully labels retinal axonal ribosomes in the SC.

2. An unbiased identification of the axonal translatome

Since the mRNA bound to the labeled axonal ribosomes of RGCs represents only a small fraction of the mRNA in the SC, a major caveat of axon-TRAP is non-specific binding of

mRNAs derived from the SC cells to immunoglobulins, Protein G and magnetic beads. To reduce this background noise, we first optimized the immunopurification protocol before performing axon-TRAP. We estimated that approximately 40% of HA-tagged translating ribosomes could be purified in this optimized protocol (Figs. 2A & S2AB, see Extended Experimental Procedures). Successful isolation of axonal ribosomes was confirmed by silver staining (Fig. S2B) followed by mass spectrometry (unpublished observation), although RpL22-HA pulled down from the SC was below the level of detection by Western blot. To assess the levels of background noise, we compared the levels of cDNAs amplified from TRAPed mRNAs (Fig. S2C) between the Cre-positive and -negative littermates. Although axon-TRAP was clearly dependent on Cre and therefore specific, additional amplification led to an increased background (Fig. 2B). We took advantage of this background "noise" reasoning that the Cre-negative samples would control for all the potential causes of false-positive signals which any technical modification could not completely eliminate.

In addition to avoiding any noise in the signal, we also wanted to assure ourselves that the signal came from mRNAs that were actively being translated, because 80S ribosomes can be stalled during translation by translational repressors such as FMRP (Darnell et al., 2011). *In vitro* ribosome run-off (see Extended Experimental Procedures) decreased the amount of TRAPed mRNAs to the degree that it could not be distinguished from the Cre-negative control (Fig. S2D), indicating that the majority of TRAPed mRNA comes from actively translating ribosomes. RNA sequencing analysis showed that we could detect 85% of TRAPed mRNAs isolated from adult axons as being actively translated (Figs. 2C & S2E). We use the term 'translatome' for ribosome-bound mRNAs in this study but it should be noted that approximately 15% of these may represent translation-stalled mRNAs.

3. Axon-TRAP identifies changing population of ribosome-bound mRNAs in developing and mature axons *in vivo*

We used axon-TRAP on SCs dissected out at three specific stages during retinotectal development and in the adult: embryonic day 17.5 (E17.5) (elongating); postnatal day 0.5 (P0.5) (branching); P7.5 (pruning); and adult (mature) (Fig. 1A). To compare the axonal translatome with the somal translatome, we also analyzed the ribosome-bound mRNAs in dissected Cre-positive retina, which contains the cell bodies of RGCs. When we plotted the normalized read count (fragments per kilobase of transcript per million mapped reads, FPKM) of each mRNA TRAPed from Cre-positive over Cre-negative SC samples, Cre-dependent signals of mRNAs were immediately visible (Fig. 2D, left panel, black dots). This was in contrast with the plot with two biological replicates of Cre-negative SC samples, which showed a clear correlation (Fig. 2D, left panel, blue dots). To select Cre-dependent mRNAs in an unbiased way, we performed “differential expression analysis” on biological replicates of Cre-positive and -negative samples using NOIseq, which is well suited for quantitative comparisons for independently performed RNA-seq samples (Tarazona et al., 2011) (Figs. 2D and S2F, see Extended Experimental Procedures). We defined these genes as “differentially expressed genes (DEGs)” (Figs. 2D & S2F, right panel, red dots) (Table S1) and used these for most of the downstream analyses.

The total number of axonally translated mRNAs was higher in early stages, peaking at P0.5, and decreased postnatally whereas mRNAs that are translated within the retinal somas showed little change over the periods examined (Fig. 2E), consistent with the amounts of axon-TRAPed cDNAs (Fig. S2A). Although previous studies demonstrated that proteins are synthesized in developing axons, it has been controversial whether mature CNS axon terminals also have an ability to synthesize proteins at all, partly because of early studies detecting few or no ribosomes in mature axons (references in (Piper and Holt, 2004)). However, the presence of DEGs, approximately 85% of which were confirmed as being translated (Figs. 2C & S2E), and ribosomes (Fig. 1IL) in adult axons indicates that axonal mRNA translation persists in adult CNS axons. The axonal translatome of RGCs is largely an evolving subset of the significantly larger somal translatome (Fig. 2F), confirming that axon-

TRAPed mRNAs originate from RGC neurons. Unlike the somal translatome (Fig. S3A), however, the axonal translatome showed extensive developmental regulation (see detailed analysis below) with only 694 out of 2576 (27%) mRNAs translating at all stages (Figs. 2G & S3A), indicating that the axonal translatome is not due to the simple passive diffusion of translating mRNAs from the soma.

4. Axon-TRAPed mRNAs encode axon-specific proteome

To discover which classes of mRNAs are preferentially translated in the axon, we performed a gene ontology (GO) enrichment/depletion analysis for genes whose translation level is significantly higher (>100-fold difference) in the axon than in the retina (Fig. 3A: "axon-enriched mRNAs"). Reassuringly, analysis with the cellular component category showed that axon-enriched mRNAs generally encode proteins that are already known to function in axons, growth cones and synapses (Figs. 3B & S3B). In contrast, mRNAs encoding nuclear proteins (e.g. modifier of chromatin structures) are depleted from axonal translatome. GO terms selectively enriched in the axonal translatome included those involved in vesicle-mediated transport and calcium-mediated signaling (Fig. S3C), suggesting that these processes, which play key roles in the distal axon, may be regulated by local mRNA translation.

To explicitly compare axonal and somal translatomes, we used ClueGO software, which reports how many genes in each cluster are assigned with specific GO terms. We compared 2576 axonally translating mRNAs ("axonal translatome") with the same number of mRNAs that are most abundant in the somal translatome but absent in the axonal translatome ("retina-only" translatome). We found that synapse- and axon-related GO terms were generally associated with the axonal translatome, while the retina-only translatome was enriched with basal body and nuclear GO terms (Fig. 3C). These results indicate the presence of mechanisms for selecting specific mRNAs for axonal translation.

5. Axonal translatome changes from axon elongation to neurotransmission during development

To correlate the local translation with the stage-specific events in axon development, we performed a GO-based analysis for genes that are translated in axons at each developmental stage using 455 neuron-related GO terms (Table S2). The translatome in younger axons (E17.5 and P0.5) was highly enriched with axon development-related GO terms, including “neuron projection morphogenesis”, whereas that of older axons (adult) was enriched with synaptic transmission-related GO terms, such as “synaptic transmission” (Figs. 4A & S4A, & Table S3). The Ingenuity Pathway Analysis (IPA) for canonical signaling pathways also suggests that synapse function was most highly regulated in adult axons (Fig. S4B). This result suggests that axonal mRNA translation continues in the mature CNS of mammals *in vivo* and may regulate presynaptic function. We found that a number of genes, which are robustly translating in adult axons, encode glutamate receptors and neurotrophin receptors (Figs. 4B & S4C), some of which are known to regulate synaptic transmission in the pre-synaptic compartment (Pinheiro and Mulle, 2008). Furthermore, key components of the trans-SNARE complex, which mediates neurotransmitter exocytosis, are highly translated in mature axons (Fig. 4B), suggesting that their local translation plays a role in supporting the core machinery of neurotransmission in pre-synapses.

Intriguingly, translation of receptors for axon guidance molecules peaks around birth (P0.5) and falls off thereafter (Figs. 4B & S4A). Because this is when interstitial branches arise from axon shafts in a topographically-biased manner to connect with targets (Fig. 1A), stage-specific synthesis of these receptors in the RGC axon may help to fine-tune topographically-biased branching. We also noted that the GO terms “neuron remodeling” and “collateral sprouting” were among most enriched in the pruning stage (P7.5). Genes with functions for synapse assembly, which include Neurexins and presynaptic cell adhesion molecules, were translating in all axons (Figs. 4B & S4A).

6. The axonal translatome changes from degenerative to survival modes at the end of development

Axon survival is regulated through at least two pathways: by maintaining axonal protein/energy homeostasis and by inhibiting a destruction program mediated by Sarm1. Sarm1, which initiates a soma-independent axon destruction program by counteracting *Nmnat* function (Gerdts et al., 2015), is highly translated in developing but not in adult axons (Figs. 4B & S4C). The same pattern of local translation was observed for caspases, whose local action mediates axon dynamics and developmentally controlled branch destruction (Campbell and Holt, 2003; Campbell and Okamoto, 2013; Simon et al., 2012). These results suggest that developing (arborizing) axons synthesize the components of axon degeneration pathways, perhaps in highly restricted subcellular compartments within the axon, for the selective withdrawal of branches, whereas adult axons shut them off to maintain mature neural connections for long periods of time.

GO terms related to mitochondrial and homeostatic functions, such as “cellular metabolism” and “mitochondrial respiratory chain”, were enriched at all stages, supporting the previous finding that axonal mRNA translation supports mitochondrial function and is required for axon survival (Figs. 4A and S4A) (Cosker et al., 2016; Hillefors et al., 2007; Yoon et al., 2012). The survival of a neuron whose axon reaches its correct target is regulated by retrograde transmission of a survival signal from the axon terminal, which turns on a transcriptional program for cell survival (Riccio et al., 1997). Previous studies showed that axonal synthesis of transcription factors, such as neurotrophin-induced synthesis of CREB (Cox et al., 2008) and SMAD1/5/8 (Ji and Jaffrey, 2012) and axon injury-induced synthesis STAT3 (Ben-Yaakov et al., 2012), regulates cell survival during development and in adulthood. Indeed, our IPA analysis revealed that components of these nuclear signaling pathways including CREB and STAT3 signaling are enriched in adult axons (Fig. S4B). Therefore, our results suggest that local translation promotes survival of mature axons both by supporting mitochondrial function and actively generating survival signals.

Pathological axon degeneration in neurodegenerative diseases has been associated with impaired axonal translation (references in (Jung et al., 2012)). A KEGG pathway enrichment analysis showed a significant over-representation of genes linked to neurodegenerative diseases such as Alzheimer's, Parkinson's and Huntington's diseases (Fig. 4A). In particular, we detected robust axonal translation of huntingtin (Htt), Prion protein (Prnp), microtubule-associated tau (Mapt), and amyloid beta precursor protein (App), whose aggregates are strongly associated with neurodegenerative disorders (Fig. 4B), suggesting a possible connection of axonal translation to neurodegeneration involving protein aggregations. Intriguingly, activating transcription factor 4 (Atf4), whose excessive axonal translation spreads Alzheimer's disease pathology across the brain (Baleriola et al., 2014), is also axonally translated at all stages tested. These results support the idea that dysregulated axonal translation may be an underlying cause of neurodegenerative diseases (Jung et al., 2012).

7. Targets of mTORC1, FMRP and APC show translational co-regulation in a stage-specific manner

We have shown that the axonal translatome is dynamically regulated during development, and this raises the important question of how axonal translation is controlled by upstream signaling pathways. To investigate this, we performed IPA upstream regulator analysis, which is based on published data of gene knockdown or knockout studies where protein products were measured when translational regulator function was impaired. mTORC1 activity was predicted to peak in actively wiring axons as its target mRNAs showed a steep increase at P0.5 (Fig. S5A), consistent with previous studies demonstrating that axonal mRNA translation is regulated by mTORC1 (Campbell and Holt, 2001) and required for axon branching (Spillane et al., 2013). In contrast, the activity of FMRP was predicted to peak later at P7.5, because its target mRNAs (whose translation is repressed) showed a coordinate decrease in translation in mature axons (Figs. 5AB & S5AB). This result suggests that the

translational brake mediated by FMRP is utilized in maturing CNS axons as in dendrites (Bagni and Greenough, 2005; Darnell and Klann, 2013). Consistent with the result, known targets of FMRP and mTORC1 in the axonal translatome showed clearly different translational patterns from the non-target mRNAs: their translation increased at P0.5 (Fig. 5A, left panel, red and blue: median shifts right) and decreased at P7.5 (right panel). Another intriguing translational regulator was APC, which was recently shown to regulate microtubule assembly and axonal growth by local translation (Preitner et al., 2014). Our analysis indicates that the translation of APC target mRNAs is highest in the youngest axons (E17.5) and steadily decreases thereafter (Fig. 5AB), consistent with the primary role of microtubule assembly in axon growth. In contrast, the targets of TDP-43 and FUS, well-known neuronal RNA-binding proteins (RBPs), showed a distribution not significantly different from the total axonal translatome (Figs. 5B & S5C), although the possibility remains that TDP-43 and FUS regulate stage-independent axonal mRNA translation. A principal component analysis (PCA) also showed a clear separation of the mTORC1, FMRP and APC targets from the rest of the axonal translatome (Fig. S5D). MicroRNAs (miRNAs) make up another class of translational regulators that function in the axon (Sasaki et al., 2014). We found that the translation of miR-1 target mRNAs decreases as the axon matures, suggesting that miR-1 abundance and/or activity increases during RGC axonal development (Fig. S5A).

We took an independent approach to investigate the possibility of developmental stage-dependent regulation of mTOR and FMRP signaling in RGC axons. We measured the abundance of phosphorylated mTOR (p-mTOR) and S6 (p-S6) in cultured primary mouse RGC axons by quantitative immunofluorescence (QIF), which positively correlate with mTORC1 activity (Copp et al., 2009; Laplante and Sabatini, 2012) (Fig. 5C). We found that they increased between E17.5 and P0.5, supporting our hypothesis that mTORC1 activity rises in RGC axons during this period. In contrast, the level of FMRP decreased in the same period, in accordance with our model that the translational brake is weakened in P0.5 axons (Fig. 5C).

To gain more insight into mRNA-specific translation in the axon, we compared the RGC axon transcriptome of E17.5 (Zivraj et al., 2010) to the axon translatome at the same stage. We analyzed the genes that are detected in the transcriptome but not in the translatome because this group may contain candidates for translationally repressed ('masked') mRNAs. We found that a significant portion of these candidates was translating at the three later stages tested (P0.5, P7.5 or adult) because their levels in the transcriptome correlated with the probability for translation at later stages (Fig. 5D). This suggests the possibility that the mRNAs, which are present in high abundance but not translating, are being stored for translation in later stages. In contrast, the genes that are present both in the young transcriptome and translatome did not show this trend (Fig. S5E).

Strikingly, mRNAs that are 'unmasked' at the same stage encode various components of specific signaling pathways (Fig. 5D). For example, components of dopamine receptor signaling, Wnt/β-catenin signaling and the oleic acid biosynthesis pathway were specifically unmasked in P0.5, P7.5 and adult axons, respectively. Additionally, as noted above, mRNAs that are unmasked at the same stage share common translational regulators (Fig. 5D). Together, these results show that functionally coherent sets of mRNAs are coordinately translated in the axon by shared upstream regulators.

8. Alternative splicing generates mRNA isoform diversity in the axon

Post-transcriptional RNA processing events, including alternative splicing, are widely used to control gene expression in neurons. To assess whether these regulate local mRNA translation, we analyzed the mRNA isoforms on mapped sequence reads using MISO software (Katz et al., 2010). Intriguingly, the axonal translatome showed more extensive diversity of mRNA isoforms than the somal translatome (Fig. 6A). To address the possibility of isoform-specific axonal translation, we selected 164 alternative events that produce two isoforms both in the axonal and retinal translatomes. Then, we calculated the 'percentage

spliced in' (PSI or Ψ) values, which represent the fraction of the longer isoform (Katz et al., 2010). Ψ_{retina} was uniformly distributed ($0< \Psi<1$) indicating that there is no clear bias in translational efficacy (Fig. 6BC). However, Ψ_{axon} was biased to the two extremes (*i.e.* $\Psi=0$ or $\Psi=1$), indicating that only one of the two isoforms is selectively translated in the axon (Fig. 6BC). Notable examples are *acot7*, an acyl-CoA thioesterase gene required for lipid biosynthesis and neuron survival (Ellis et al., 2013), *syntaxin 3* (*stx3*), a SNARE component gene, and *clta*, a clathrin light chain A gene, which show clear axon-specific usage of first, last and internal exons, respectively (Figs. 6DE & S6A). Intriguingly, axon-specific isoforms of *acot7* and *stx3* encode proteins with slightly different amino acids at the N- and C-termini, respectively (see gene models in Fig. 6DE), suggesting that alternative splicing may couple axon-specific protein isoforms with a unique sequence tag in the UTR.

Unexpectedly, we detected a number of back splicing events for three genes (*Rhobtb3*, *Ubn2* and *Ankrd12*), which indicate the potential presence of circRNAs in the axonal but not in the retinal translatome, and we could detect these mRNAs by RT-PCR of unamplified axonal translatome (Fig. S6B). Although previous studies suggested that the circRNAs are not translated (Guo et al., 2014), our result raises the possibility that the ribosomes can associate with circRNAs in axons. However, further studies are needed to address whether proteins are actually synthesized from these circRNAs.

9. *Cis*-regulatory elements couple alternative splicing with axonal translation

The dominance of a single alternative exon in axons suggests that axonal mRNA translation might be mechanistically linked to alternative splicing. We focused on the axonally enriched mRNAs with an alternative first or last exon because 5'- and 3'-UTRs generally contain localization signals (references in (Jung et al., 2012)) (Fig. 6DE). In order to investigate whether the axon-specific exons are sufficient to promote axonal mRNA transport and translation, we used a diffusion-limited, membrane-targeted EGFP (myr-d2EGFP), which is a faithful reporter of local protein synthesis in dendrites (Aakalu et al., 2001) and in axons

(Andreassi et al., 2010; Cox et al., 2008). We fused the axon-specific or axon-absent (retina-restricted) alternative exon of each gene to myr-d2EGFP so that a reporter mRNA containing each motif would be generated in cells (Fig. 7AB). To test these reporters in retinal ganglion cells, the same cell-type from which they were identified, we used *Xenopus* primary retinal cultures (Campbell and Holt, 2001), which is amenable to screening multiple motifs. We confirmed that alternative usages of 5'- and 3'- UTRs of *acot7* and *stx3*, respectively, are conserved between mouse and Xenopus (Xenbase and UCSC genome browser). Fluorescence recovery after photobleaching (FRAP) was monitored in the growth cones of cultured RGCs at 1 min intervals for 10 min. Remarkably, the axon-specific isoforms showed rapid and robust FRAP signal whereas the retina-specific isoforms did not (Fig. 7AB). These results indicate that axon-specific exons of *acot7* and *stx3* are sufficient to promote axonal mRNA translation (Fig. 7AB).

We next investigated whether axon-specific exons might contain 'generalizable' motifs responsible for axonal mRNA translation. We searched for common sequence elements that are enriched in axon-specific alternatively exons (Fig. 7C) and in the 5'- and 3'-UTRs in constitutive exons (Fig. S7AB) of axon-enriched mRNAs (Fig. 3A). To understand the potential function of identified sequence elements, we searched for genes that contain these elements in the entire mouse genome. Remarkably, the element-containing genes generally encode regulators of axon and synapse function (Figs. 7C & S7C). Strikingly, five of six motifs identified from alternative exons and five of twelve motifs in constitutive exons of axon-enriched mRNAs showed significant a FRAP signal at 10 min indicative of increased axonal mRNA translation of a reporter mRNA when incorporated in the 5' or 3'-UTR as in Figure 7B (Figs. 7C & S7C). These results suggest the potential links between the sequence elements and axonal mRNA translation, and thus provide further insight into the mechanisms underlying the selective and dynamic nature of the axonal mRNA translation.

DISCUSSION

Here, we developed a mouse model of axon-TRAP to isolate mRNAs translating in the distal axon of RGCs *in vivo* and performed a genome-wide survey of the axonal translatome at critical time points during the assembly of visual circuitry and in adulthood. The axonal translatome is generally a subpopulation of its somal counterpart but is enriched in genes with axon-specific roles. We found that broadly two classes of local translatomes exist in the distal axon, one being constitutively translated and the other being developmentally regulated. The former generally encodes the regulators of protein and energy homeostasis and the latter encodes proteins required for stage-specific events, such as axon elongation, axon branching, synapse formation and synaptic transmission. The adult axonal translatome is unique and its main role is likely to regulate synapse function. Developmentally regulated translatomes were subdivided according to the changes in translation between stages, and those that showed a coordinate change were found to share common upstream regulators, such as mTORC1, FMRP and APC as well as novel sequence elements that possibly regulate axonal mRNA translation. Additionally, we found that axonally translated mRNAs were frequently specific splice variants that carried axon-specific motifs. Together, our results show that extensive local mRNA translation occurs in the developing and mature mammalian CNS axons *in vivo*, and provide strong evidence that highly regulated axonal mRNA translation might be at the heart of CNS development and the maintenance of synaptic function.

Previous studies using cultured neurons have revealed that some mRNAs are stored in a translationally repressed state (Buxbaum et al., 2014; Graber et al., 2013). Two independent and complementary approaches have been developed to ask which mRNAs are translating in the axon (Kim and Jung, 2015): metabolic labeling of newly synthesized proteins and isolation of ribosome-bound mRNAs. Proteomic approaches provide the ultimate readout of gene expression as they can identify post-translationally modified protein products, but a critical limitation of proteomics is that the probe – tagged amino acid or its analogs label all

cells, limiting its use to compartmentalized axon culture. An alternative strategy to identify newly synthesized proteins is to look at translating mRNAs (translatome), because these are the obligate precursor to the *de novo* proteome. A key advantage of this approach is that ribosomes can be isolated from a specific cell type, by expressing a genetically encoded epitope-tagged ribosomal protein in just the cells of interest (TRAP) (Heiman et al., 2008). Isolated ribosome-mRNA complexes either can be partially digested by RNase, and the fragments protected by ribosome binding can be sequenced ("Ribosome profiling") (Ingolia et al., 2011), or the entire mRNA can be separated from the ribosome and directly sequenced. Only the latter method, which we use in this study, allows the discovery of novel isoforms outside the protein-coding region.

We compared translatomes of RGC axons and retinal cell bodies in the same animals. It should be noted that the retinal translatome includes the translatome of the short axons and dendrites of the intraretinal circuitry, as well as their cell bodies. Therefore, the number of mRNAs that are identified as selectively translating in the axon in this study may be an underestimation. Additionally, the expression of tagged-ribosomes in non-RGC retinal neurons can potentially introduce bias into the axon/soma ratio. However, given the previous observations on retinal cell populations (Young, 1985), the presence of non-RGC mRNAs in the retinal sample cannot explain the axonal enrichment of mRNAs above the threshold ($FPKM_{axon}$ / $FPKM_{retina}$ > 100), which we used for the axon-soma comparison. The strong enrichment of genes with axonal function in the axonal translatome compared to the retinal translatome suggests that these mRNAs were disproportionately represented in the axonal translatome, indicating that that axonal translation is mRNA-specific.

In this study, we show that the RGC axonal translatome changes in a developmental stage-specific manner, in such a way that proteins playing a key role at specific periods are synthesized when needed. This result is in agreement with a recent study using the *Drosophila* visual system, which reported that neuronal differentiation associated with

maturation of presynaptic terminals is regulated by coordinate control of mRNA translation (Zhang et al., 2016), although the subcellular location of mRNA translation was not addressed in that study. Whether signals that regulate mRNA-specific translation come from a cell-intrinsic timer or cell-extrinsic cues remains to be investigated, but our bioinformatic and experimental analyses suggest that this involves stage-dependent activation of RNA-binding proteins, including FMRP. Because FMRP is known to inhibit translation of proteins required for synapse formation and its loss of function leads to over-branching of central nervous system axons (references in (Darnell and Richter, 2012)), it is reasonable to assume that FMRP may be activated after CNS axons make appropriate synapses to limit the number of synapses that a single axon makes. In this sense, it is intriguing that defective translational machinery, which is expected to affect all cells in the organism, leads to enigmatically synapse-specific phenotypes ranging from defective synaptic transmission to impaired cognitive function and memory (references in (Buffington et al., 2014)). Although the subcellular location of this pathogenesis is unknown, it will be interesting to test whether the axonal translatome of developing cortical neuronal axons in these mouse models of neurodevelopmental disorders is any different from normal mice.

The local mRNA translation in axons of mature neurons has been a subject of long-standing debate (Piper and Holt, 2004). Evidence indicates that ribosomes exist in mature CNS axons (Koenig et al., 2000; Kun et al., 2007; Walker et al., 2012) and that their number is dynamically regulated under normal and pathological conditions (Verheijen et al., 2014). However, what proteins are locally translating in the mature axons was unknown. Our comparative analysis of mature and developing retinal axonal translatomes suggest that local protein synthesis regulates synaptic transmission and axon maintenance. Because axonal translation has been implicated in axonal survival and degeneration (Jung et al., 2012), it will be important to find out whether pathological axon degeneration is preceded by defective axonal translation. The power of axon-TRAP is that it can be extended to other neurons whose cell bodies and axons are anatomically separated. One such example is cortical and

spinal motor neurons, whose axonal degeneration leads to human diseases such as amyotrophic lateral sclerosis (ALS). Recent evidence suggests that defective axonal mRNA transport and translation may be an underlying cause of ALS pathology (Alami et al., 2014; Murakami et al., 2015). Our new technical approach and datasets should provide a valuable resource for future studies.

EXPERIMENTAL PROCEDURES

Histological analysis

For immunohistochemistry, tissue sections (12 μm) were visualized using an anti-HA antibody (Abcam ab9110) and a secondary antibody conjugated to Alexa Fluor 488 (Life technologies). For immuno-gold electron microscopy, tissues were fixed in 4% paraformaldehyde in 0.1M HEPES (pH 7.4), and the HA-tagged ribosomes were visualized by the same anti-HA antibody and IgG conjugated with gold (10nm-15nm). Mouse RGC axon culture and quantitative immunofluorescence were performed as previously described (Zivraj et al., 2010) using the following antibodies: anti-mTOR (phospho S2448) antibody (Abcam 109268), anti-FMRP antibody (Abcam 17722), and anti-RPS6 (phospho S235 + S236) antibody (Abcam 12864).

Axon-Translating Ribosome Affinity Purification (TRAP)

A homozygote RiboTag female mouse was mated with a Pax6-alpha-Cre male, to produce Cre-positive and Cre-negative mice in a single litter. Three eyes or six SCs were homogenized and post-mitochondrial fractions were collected. The mRNA-ribosome complexes were precipitated using the polyclonal HA antibody and Dynabeads Protein G (Life Technologies 10004D). For the *in vitro* ribosome run-off experiments, TRAP was performed after lysate was incubated with rabbit reticulocyte lysate (Promega), harringtonine (Sigma) and 4E1RCat (Sigma) at 37°C for 30 min. Ribosome-bound mRNAs were amplified

by a method developed by Tang and colleagues (Tang et al., 2009) with slight modification and sequenced using Illumina HiSeq2000 or NextSeq500.

Data analysis

The sequence reads were mapped using TopHat 2 version 2.0.12 and FPKM values were estimated using Cufflinks. Read counts for each gene were determined using HTSeq version 0.6.1p1. For the identification of translated mRNAs in RGC axons, we applied the differential gene expression analysis on read count using NOISeq. *De novo* motif analysis was performed using HOMER version 3.0 with custom FASTA files. All RNA-seq data are deposited in Gene Expression Omnibus (GEO) datasets under accession number GSE79352.

A detailed description of all experimental procedures is provided in the Supplemental Information.

AUTHOR CONTRIBUTIONS

HJ and CEH conceived and supervised the project. HJ performed histological experiments. HJ and TS performed biochemical and molecular biological experiments. TS performed bioinformatic analyses. JJ performed Cre specificity experiments, JO performed motif imaging and QIF, and BT-B and JQL performed FRAP and QIF. PSA provided RiboTag mice and the original TRAP protocol. HJ, TS and CEH wrote the manuscript.

ACKNOWLEDGEMENTS

We apologize authors of key papers, which we could not cite due to space limitations. We thank W. Harris for many valuable discussions and critical reading of the manuscript. We thank A. Riccio for myr-d2EGFP, J. Skepper for EM, Gihoon Son for advice on IPA, M. Minett for advice on mouse genetics, K. Mooslerhner, A. Dwivedy, Jeeun Song for technical assistance. This work was supported by Wellcome Trust Programme Grant (085314/Z/08/Z),

European Research Council Advanced Grant (322817) to CEH, Cambridge Wellcome Trust PhD programme in Developmental Biology (PMAG/406; BT-B), Gates Cambridge Scholarship (JQL), Basic Science Research Program (2013R1A1A1009625 & 2014K2A7A1036305), Biomedical Technology Development Program (2013M3A9D5072551), & Brain Research Program (2015M3C7A1028396) funded through the NRF by the Korean government (MSIP), Yonsei University Future-leading Research Initiative of 2015 (2015-22-0095), and a faculty research grant from Yonsei University College of Medicine for 2013 (6-2013-0064-2-1) to HJ.

REFERENCES

Aakalu, G., Smith, W.B., Nguyen, N., Jiang, C., and Schuman, E.M. (2001). Dynamic visualization of local protein synthesis in hippocampal neurons. Neuron *30*, 489-502.

Alami, N.H., Smith, R.B., Carrasco, M.A., Williams, L.A., Winborn, C.S., Han, S.S., Kiskinis, E., Winborn, B., Freibaum, B.D., Kanagaraj, A.*, et al.* (2014). Axonal transport of TDP-43 mRNA granules is impaired by ALS-causing mutations. Neuron *81*, 536-543.

Andreassi, C., Zimmermann, C., Mitter, R., Fusco, S., Devita, S., Saiardi, A., and Riccio, A. (2010). An NGF-responsive element targets myo-inositol monophosphatase-1 mRNA to sympathetic neuron axons. Nat Neurosci *13*, 291-301.

Bagni, C., and Greenough, W.T. (2005). From mRNP trafficking to spine dysmorphogenesis: the roots of fragile X syndrome. Nat Rev Neurosci *6*, 376-387.

Baleriola, J., Walker, C.A., Jean, Y.Y., Crary, J.F., Troy, C.M., Nagy, P.L., and Hengst, U. (2014). Axonally synthesized ATF4 transmits a neurodegenerative signal across brain regions. Cell *158*, 1159-1172.

Ben-Yaakov, K., Dagan, S.Y., Segal-Ruder, Y., Shalem, O., Vuppalanchi, D., Willis, D.E., Yudin, D., Rishal, I., Rother, F., Bader, M.*, et al.* (2012). Axonal transcription factors signal retrogradely in lesioned peripheral nerve. EMBO J *31*, 1350-1363.

Brunet, I., Weinl, C., Piper, M., Trembleau, A., Volovitch, M., Harris, W., Prochiantz, A., and Holt, C. (2005). The transcription factor Engrailed-2 guides retinal axons. Nature *438*, 94-98.

Buffington, S.A., Huang, W., and Costa-Mattioli, M. (2014). Translational control in synaptic plasticity and cognitive dysfunction. Annu Rev Neurosci *37*, 17-38.

Buxbaum, A.R., Wu, B., and Singer, R.H. (2014). Single beta-actin mRNA detection in neurons reveals a mechanism for regulating its translatability. Science *343*, 419-422.

Campbell, D.S., and Holt, C.E. (2001). Chemotropic responses of retinal growth cones mediated by rapid local protein synthesis and degradation. Neuron *32*, 1013-1026.

Campbell, D.S., and Holt, C.E. (2003). Apoptotic pathway and MAPKs differentially regulate chemotropic responses of retinal growth cones. Neuron *37*, 939-952.

Campbell, D.S., and Okamoto, H. (2013). Local caspase activation interacts with Slit-Robo signaling to restrict axonal arborization. J Cell Biol *203*, 657-672.

Copp, J., Manning, G., and Hunter, T. (2009). TORC-specific phosphorylation of mammalian target of rapamycin (mTOR): phospho-Ser2481 is a marker for intact mTOR signaling complex 2. Cancer Res *69*, 1821-1827.

Cosker, K.E., Fenstermacher, S.J., Pazyra-Murphy, M.F., Elliott, H.L., and Segal, R.A. (2016). The RNA-binding protein SFPQ orchestrates an RNA regulon to promote axon viability. Nat Neurosci.

Cox, L.J., Hengst, U., Gurskaya, N.G., Lukyanov, K.A., and Jaffrey, S.R. (2008). Intra-axonal translation and retrograde trafficking of CREB promotes neuronal survival. Nat Cell Biol.

Darnell, J.C., and Klann, E. (2013). The translation of translational control by FMRP: therapeutic targets for FXS. Nat Neurosci *16*, 1530-1536.

Darnell, J.C., and Richter, J.D. (2012). Cytoplasmic RNA-binding proteins and the control of complex brain function. Cold Spring Harb Perspect Biol *4*, a012344.

Darnell, J.C., Van Driesche, S.J., Zhang, C., Hung, K.Y., Mele, A., Fraser, C.E., Stone, E.F., Chen, C., Fak, J.J., Chi, S.W.*, et al.* (2011). FMRP stalls ribosomal translocation on mRNAs linked to synaptic function and autism. Cell *146*, 247-261.

Ellis, J.M., Wong, G.W., and Wolfgang, M.J. (2013). Acyl coenzyme A thioesterase 7 regulates neuronal fatty acid metabolism to prevent neurotoxicity. Mol Cell Biol *33*, 1869-1882.

Feldheim, D.A., and O'Leary, D.D. (2010). Visual map development: bidirectional signaling, bifunctional guidance molecules, and competition. Cold Spring Harbor perspectives in biology *2*, a001768.

Gerdts, J., Brace, E.J., Sasaki, Y., DiAntonio, A., and Milbrandt, J. (2015). Neurobiology. SARM1 activation triggers axon degeneration locally via NAD(+) destruction. Science *348*, 453-457.

Godement, P., Salaun, J., and Imbert, M. (1984). Prenatal and postnatal development of retinogeniculate and retinocollicular projections in the mouse. J Comp Neurol *230*, 552-575.

Graber, T.E., Hebert-Seropian, S., Khoutorsky, A., David, A., Yewdell, J.W., Lacaille, J.C., and Sossin, W.S. (2013). Reactivation of stalled polyribosomes in synaptic plasticity. Proc Natl Acad Sci U S A *110*, 16205-16210.

Guo, J.U., Agarwal, V., Guo, H., and Bartel, D.P. (2014). Expanded identification and characterization of mammalian circular RNAs. Genome biology *15*, 409.

Heiman, M., Schaefer, A., Gong, S., Peterson, J.D., Day, M., Ramsey, K.E., Suarez-Farinas, M., Schwarz, C., Stephan, D.A., Surmeier, D.J.*, et al.* (2008). A translational profiling approach for the molecular characterization of CNS cell types. Cell *135*, 738-748.

Hillefors, M., Gioio, A.E., Mameza, M.G., and Kaplan, B.B. (2007). Axon viability and mitochondrial function are dependent on local protein synthesis in sympathetic neurons. Cell Mol Neurobiol *27*, 701-716.

Holt, C.E., and Schuman, E.M. (2013). The central dogma decentralized: new perspectives on RNA function and local translation in neurons. Neuron *80*, 648-657.

Ingolia, N.T., Lareau, L.F., and Weissman, J.S. (2011). Ribosome profiling of mouse embryonic stem cells reveals the complexity and dynamics of mammalian proteomes. Cell *147*, 789-802.

Ji, S.J., and Jaffrey, S.R. (2012). Intra-axonal translation of SMAD1/5/8 mediates retrograde regulation of trigeminal ganglia subtype specification. Neuron *74*, 95-107.

Jung, H., Yoon, B.C., and Holt, C.E. (2012). Axonal mRNA localization and local protein synthesis in nervous system assembly, maintenance and repair. Nat Rev Neurosci *13*, 308-324.

Katz, Y., Wang, E.T., Airoldi, E.M., and Burge, C.B. (2010). Analysis and design of RNA sequencing experiments for identifying isoform regulation. Nature methods *7*, 1009-1015.

Kim, E., and Jung, H. (2015). Local protein synthesis in neuronal axons: why and how we study. BMB reports *48*, 139-146.

Koenig, E., Martin, R., Titmus, M., and Sotelo-Silveira, J.R. (2000). Cryptic peripheral ribosomal domains distributed intermittently along mammalian myelinated axons. J Neurosci *20*, 8390-8400.

Kun, A., Otero, L., Sotelo-Silveira, J.R., and Sotelo, J.R. (2007). Ribosomal distributions in axons of mammalian myelinated fibers. J Neurosci Res *85*, 2087-2098.

Laplante, M., and Sabatini, D.M. (2012). mTOR signaling in growth control and disease. Cell *149*, 274-293.

Marquardt, T., Ashery-Padan, R., Andrejewski, N., Scardigli, R., Guillemot, F., and Gruss, P. (2001). Pax6 is required for the multipotent state of retinal progenitor cells. Cell *105*, 43-55.

Martin, K.C., and Ephrussi, A. (2009). mRNA localization: gene expression in the spatial dimension. Cell *136*, 719-730.

Murakami, T., Qamar, S., Lin, J.Q., Schierle, G.S., Rees, E., Miyashita, A., Costa, A.R., Dodd, R.B., Chan, F.T., Michel, C.H.*, et al.* (2015). ALS/FTD Mutation-Induced Phase Transition of FUS Liquid Droplets and Reversible Hydrogels into Irreversible Hydrogels Impairs RNP Granule Function. Neuron.

Pinheiro, P.S., and Mulle, C. (2008). Presynaptic glutamate receptors: physiological functions and mechanisms of action. Nat Rev Neurosci *9*, 423-436.

Piper, M., and Holt, C. (2004). RNA translation in axons. Annu Rev Cell Dev Biol *20*, 505-523.

Preitner, N., Quan, J., Nowakowski, D.W., Hancock, M.L., Shi, J., Tcherkezian, J., Young-Pearse, T.L., and Flanagan, J.G. (2014). APC is an RNA-binding protein, and its interactome provides a link to neural development and microtubule assembly. Cell *158*, 368-382.

Riccio, A., Pierchala, B.A., Ciarallo, C.L., and Ginty, D.D. (1997). An NGF-TrkA-mediated retrograde signal to transcription factor CREB in sympathetic neurons. Science *277*, 1097-1100.

Sanz, E., Yang, L., Su, T., Morris, D.R., McKnight, G.S., and Amieux, P.S. (2009). Cell-type-specific isolation of ribosome-associated mRNA from complex tissues. Proc Natl Acad Sci U S A *106*, 13939-13944.
Sasaki, Y., Gross, C., Xing, L., Goshima, Y., and Bassell, G.J. (2014). Identification of axon-enriched microRNAs localized to growth cones of cortical neurons. Dev Neurobiol *74*, 397-406.
Simon, D.J., Weimer, R.M., McLaughlin, T., Kallop, D., Stanger, K., Yang, J., O'Leary, D.D., Hannoush, R.N., and Tessier-Lavigne, M. (2012). A caspase cascade regulating developmental axon degeneration. J Neurosci *32*, 17540-17553.
Spillane, M., Ketschek, A., Merianda, T.T., Twiss, J.L., and Gallo, G. (2013). Mitochondria coordinate sites of axon branching through localized intra-axonal protein synthesis. Cell reports *5*, 1564-1575.
Tang, F., Barbacioru, C., Wang, Y., Nordman, E., Lee, C., Xu, N., Wang, X., Bodeau, J., Tuch, B.B., Siddiqui, A.*, et al.* (2009). mRNA-Seq whole-transcriptome analysis of a single cell. Nat Methods *6*, 377-382.
Tarazona, S., Garcia-Alcalde, F., Dopazo, J., Ferrer, A., and Conesa, A. (2011). Differential expression in RNA-seq: a matter of depth. Genome research *21*, 2213-2223.
Verheijen, M.H., Peviani, M., Hendricusdottir, R., Bell, E.M., Lammens, M., Smit, A.B., Bendotti, C., and van Minnen, J. (2014). Increased axonal ribosome numbers is an early event in the pathogenesis of amyotrophic lateral sclerosis. PLoS One *9*, e87255.
Walker, B.A., Hengst, U., Kim, H.J., Jeon, N.L., Schmidt, E.F., Heintz, N., Milner, T.A., and Jaffrey, S.R. (2012). Reprogramming axonal behavior by axon-specific viral transduction. Gene Ther *19*, 947-955.
Yoon, B.C., Jung, H., Dwivedy, A., O'Hare, C.M., Zivraj, K.H., and Holt, C.E. (2012). Local Translation of Extranuclear Lamin B Promotes Axon Maintenance. Cell *148*, 1-13.
Young, R.W. (1985). Cell differentiation in the retina of the mouse. Anat Rec *212*, 199-205.
Zhang, K.X., Tan, L., Pellegrini, M., Zipursky, S.L., and McEwen, J.M. (2016). Rapid Changes in the Translatome during the Conversion of Growth Cones to Synaptic Terminals. Cell reports *14*, 1258-1271.
Zivraj, K.H., Tung, Y.C., Piper, M., Gumy, L., Fawcett, J.W., Yeo, G.S., and Holt, C.E. (2010). Subcellular profiling reveals distinct and developmentally regulated repertoire of growth cone mRNAs. J Neurosci *30*, 15464-15478.

FIGURE LEGENDS

Figure 1. Retinal RiboTag labels RGC axonal ribosomes *in vivo*. (A) Development of retinal ganglion cell (RGC) axons in the superior colliculus (SC). **(B)** Strategy of axon-TRAP. **(C)** PCR that detects *Cre* transgene (upper) and *rpL22* allele (lower). **(D)** PCR of genomic DNA from the retina and the SC that distinguish recombined and unrecombined RiboTag alleles. **(E)** HA fluorescence immunohistochemistry. **(F-L)** HA immunogold electron microscopy (EM)**.** HA-tagged ribosomes localize to retinal cell bodies (F), and RGC axons (Ax) in the optic nerve head (ONH) (H), optic nerve (ON) (I) and RGC axon terminals in the SC (J-K). Two or more adjacent gold particles (purple arrows) were regarded as specific

signals. Scattered single immunogold particles may be nonspecific (yellow asterisks). Ultrastructure of polysomes is visible in the cell bodies in the retina and the SC (white arrows), but these co-localize with immunogold only in the retina (F). E: embryonic day; P: postnatal day; Nuc: nucleus. Scale bars: 500 μm (E) and 500 nm (F-L).

Figure 2. Unbiased identification of the axonal translatome. (A) HA-labeled ribosomes were TRAPed by two independent antibodies against HA, and then co-immunoprecipitated ribosomal proteins from 60S (*i.e.* rpL24) and 40S (*i.e.* rpS3a) were visualized by Western blot. IgG LC, immunoglobulin G light chain. **(B)** Double strand cDNAs were made from TRAPed RNAs. **(C)** A scatterplot of log2 (FPKM) between Cre-positive/-negative (x axis) and Cre-negative axons (y axis). **(D)** Read counts of adult SC samples with or without ribosome run-off. Left panel is a scatter plot of $\log_2$ (read count+1) and right panel represents the percentage of genes whose read counts were decreased by run-off. **(E)** Change in numbers of DEGs in the retina and axon. For axon, dark pink indicates DEGs at the corresponding stages. Light pink indicates genes which are DEGs only at that stage. Combined value of orange and peach (union of DEGs) indicates the size of axonal translatome. **(F)** Somal versus axonal translatomes. **(G)** Four different axonal translatomes.

Figure 3. Comparison between the axonal and retinal translatomes (A) Normalized mRNA levels ($\log_2$(FPKM)) between the axonal (y axis) and retinal (x axis) translatome at stage P0.5. Axon- and retina-enriched population were defined when $FPKM_{axon}$ / $FPKM_{retina}$ > 100 and < 0.1, respectively. **(B)** GO terms in the cellular component category. More detailed lists are in Fig. S3B (grey, not detected). **(C)** ClueGO analysis. The left axis indicates the parental GO terms. The percentage of daughter GO terms associated with somal and axonal translatome is presented.

Figure 4. Developmental changes of translated genes in RGC axons (A) Enriched GO (biological process) terms and KEGG pathways for axonally translated genes, sorted by

significance for each stage (Fisher's exact test). The enrichment was analyzed by topGO (Table S3). Statistically significant cells are marked by black squares. **(B)** Normalized levels of axonal translation for selected genes (grey, not detected).

Figure 5. *Trans*-acting elements that regulate the axonal translatome (A) Density plots of the change in FPKM values of axonal translatomes during two consecutive developmental stages (log2(stage A(FPKM) / stage B (FPKM)) (grey, distribution of all genes; colors, distribution of target genes) with p-values (Kolmogorov-Smirnov test). **(B)** Average log2 (FPKM) values of target genes (mean±95% confidence interval). **(C)** Representative immunofluorescence images (left) and their quantification (right) (mean±SEM). ***p<0.001, Mann-Whitney test. Scale bar, 10 μm. **(D)** Relationship between transcript abundance of the genes not detected in E17.5 axonal translatome (read count = 0) and probability of their translation at later stages (upper left: blue line, mRNA level in transcriptome; red line, moving averages of percentage of genes detected at any of three later stages over a window size of 100 genes; r, Pearson correlation coefficient). The upper right and lower heatmaps show mRNA abundance in the translatome and enriched regulators/pathways, respectively.

Figure 6. Alternative splicing generates high isoform diversity in axons. (A) Percentage of genes with alternative events from all axonally translated genes. Alternative events are classified into 5 different classes depicted in the left panel. **(B)** Scatter and density plots for the distribution of Percentage Spliced In (Ψ) values between the retina (x-axis) and the axon (y-axis). **(C)** Model for biased distribution of Ψ values in the axon. The comparison of two isoforms suggests that one of two isoforms is predominant in the axon. **(D-E)** The sequence reads on *acot7* and *stx3* loci visualized by Integrative Genomics Viewer (IGV). The histograms show the depth of the reads displayed at each locus. The retinal isoforms detected only in the retinal translatome, whereas the axonal isoforms are detected both in the axonal and retinal translatomes.

Figure 7. *Cis*-regulatory elements link alternative splicing to axonal translation.

(A-B) Axon- and retina-specific *acot7* and *stx3* UTR isoforms fused with myr-d2EGFP were expressed in cultured RGCs (Xenopus). Quantification of fluorescence intensity after photobleaching (FRAP) revealed axon-specific isoforms of *acot7* (A) and *stx3* (B) markedly increase axonal translation of the myr-d2EGFP reporter construct compared to retina-specific UTR counterparts. Data at each 1 min timepoint represent mean fraction of recovery relative to pre- and post-bleach levels ±SEM. (*n*= 9 and 10 for axon and eye-specific 5'UTR of *acot7*, respectively; *n* = 14 and 14 for axon and eye-specific 3'UTR of *stx3,* respectively*).* ***p<0.0001, two-way ANOVA. FRAP signal recovery was abolished by 40μM anisomycin (10 min post-photobleach: acot7 axon-isoform + anisomycin 0.064 ± 0.028; Stx3 axon-isoform + anisomycin 0.085 ± 0.026). Representative images of RGC axonal growth cones showing fluorescent recovery after photobleaching for each reporter construct are shown (right). Scale bars, 10 μm. **(C)** GO enrichment analysis for entire genome containing axon-specific sequence motifs associated with alternative exons (S: G or C) and their relative efficiency in axonal mRNA translation using myr-d2EGFP reporter constructs. Significance of FRAP recovery curves were compared to no UTR control across 10 min (*n* ≥ 10 for each construct). Statistical significance of FRAP compared to the no-UTR control was tested across all time-points (1-10 min) using a two-way ANOVA (*** p<0.0001 compared to no-UTR control). For representative purposes, the mean fluorescence recovery at 10 min post-photobleaching is shown. Error bars represent SEM.

Figure 1

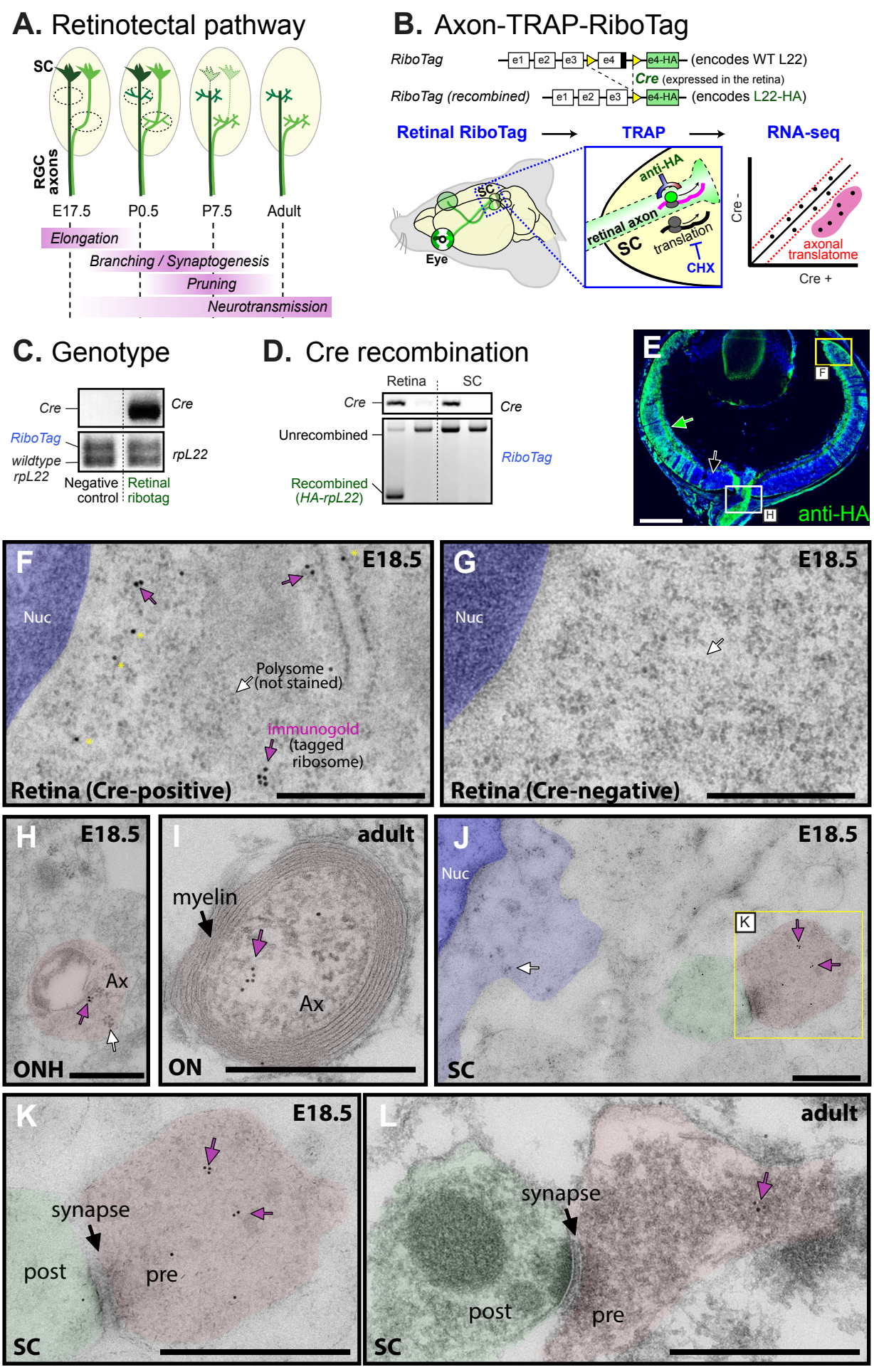

Figure 2

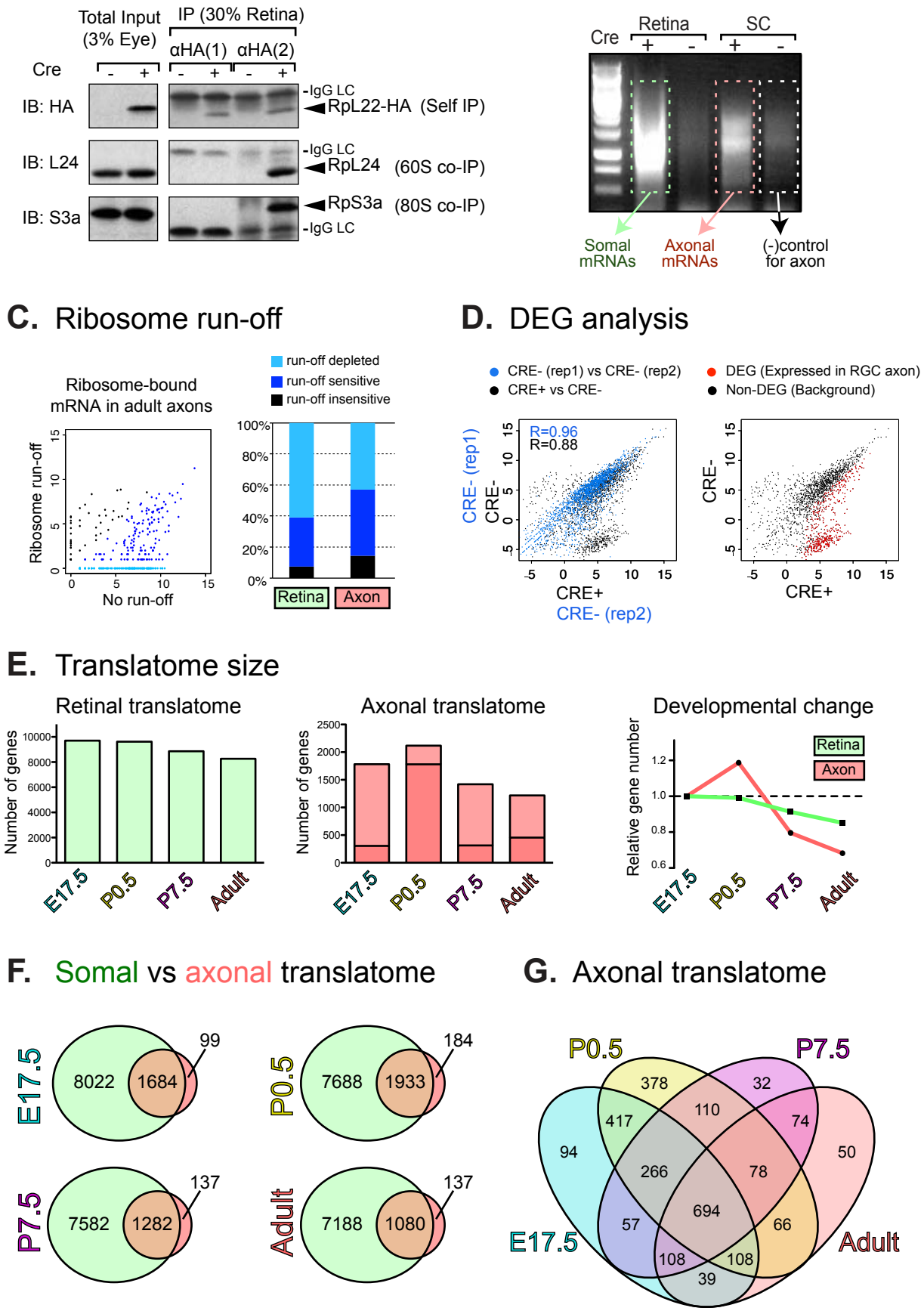

Figure 3

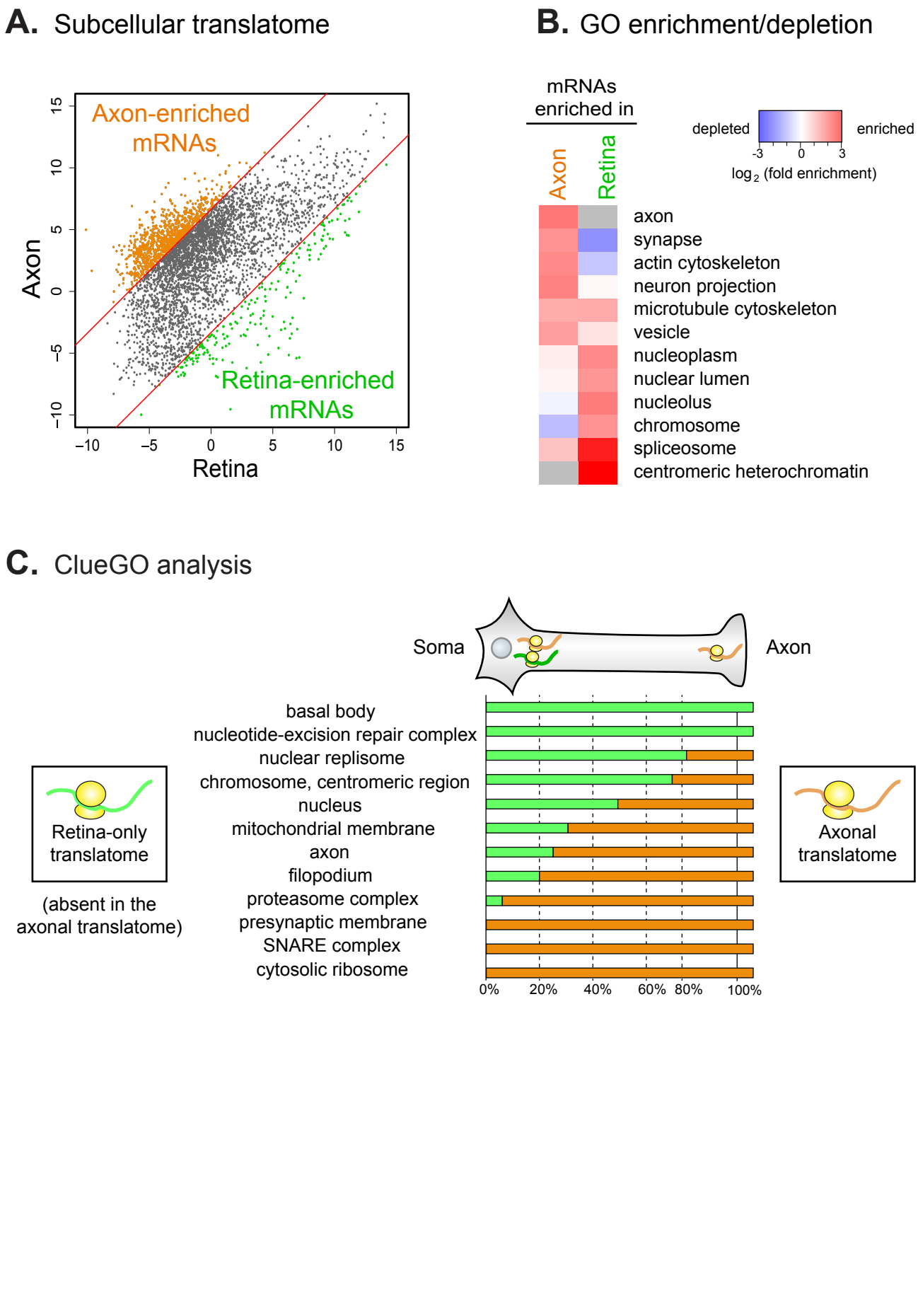

Figure 4

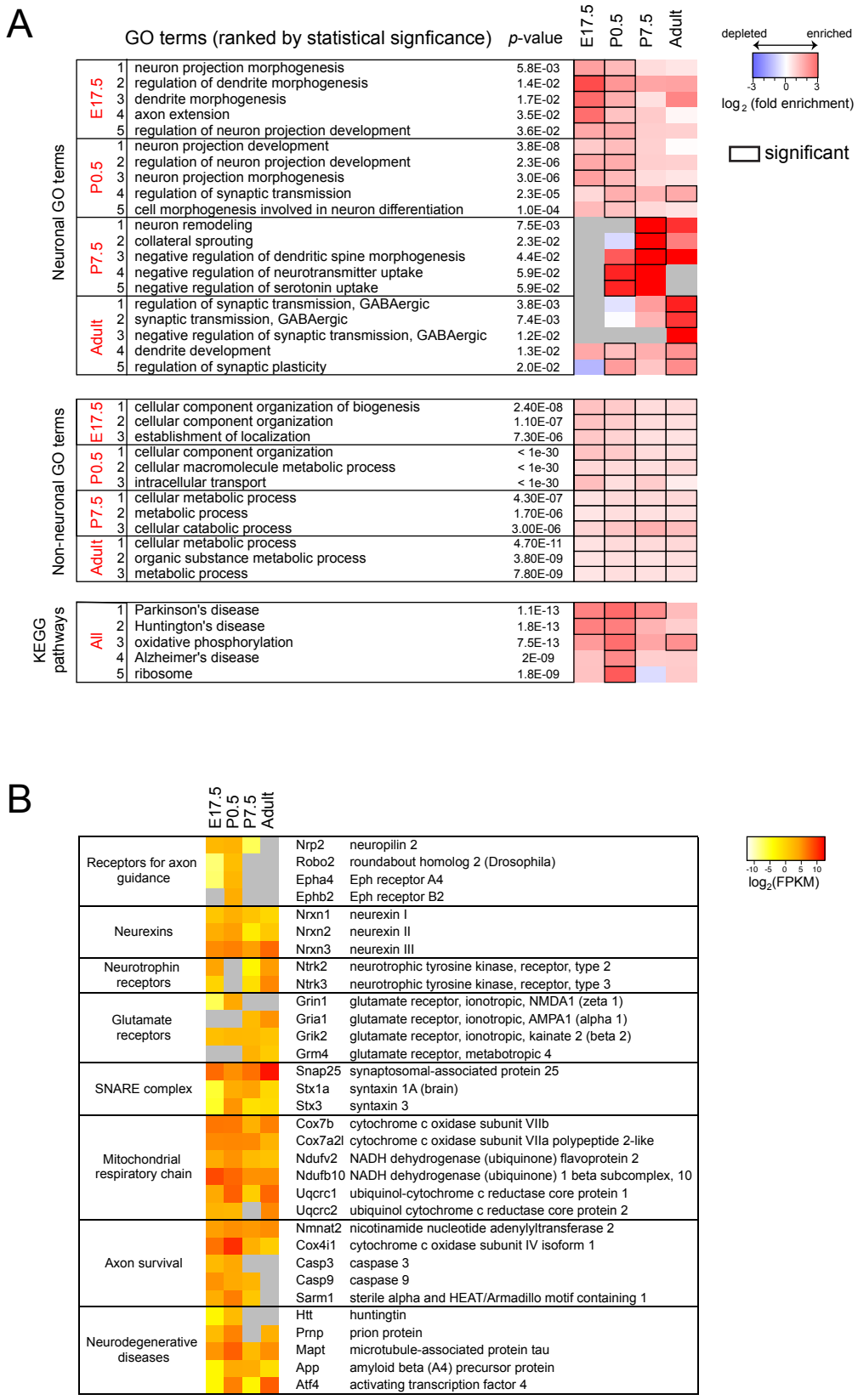

Figure 5

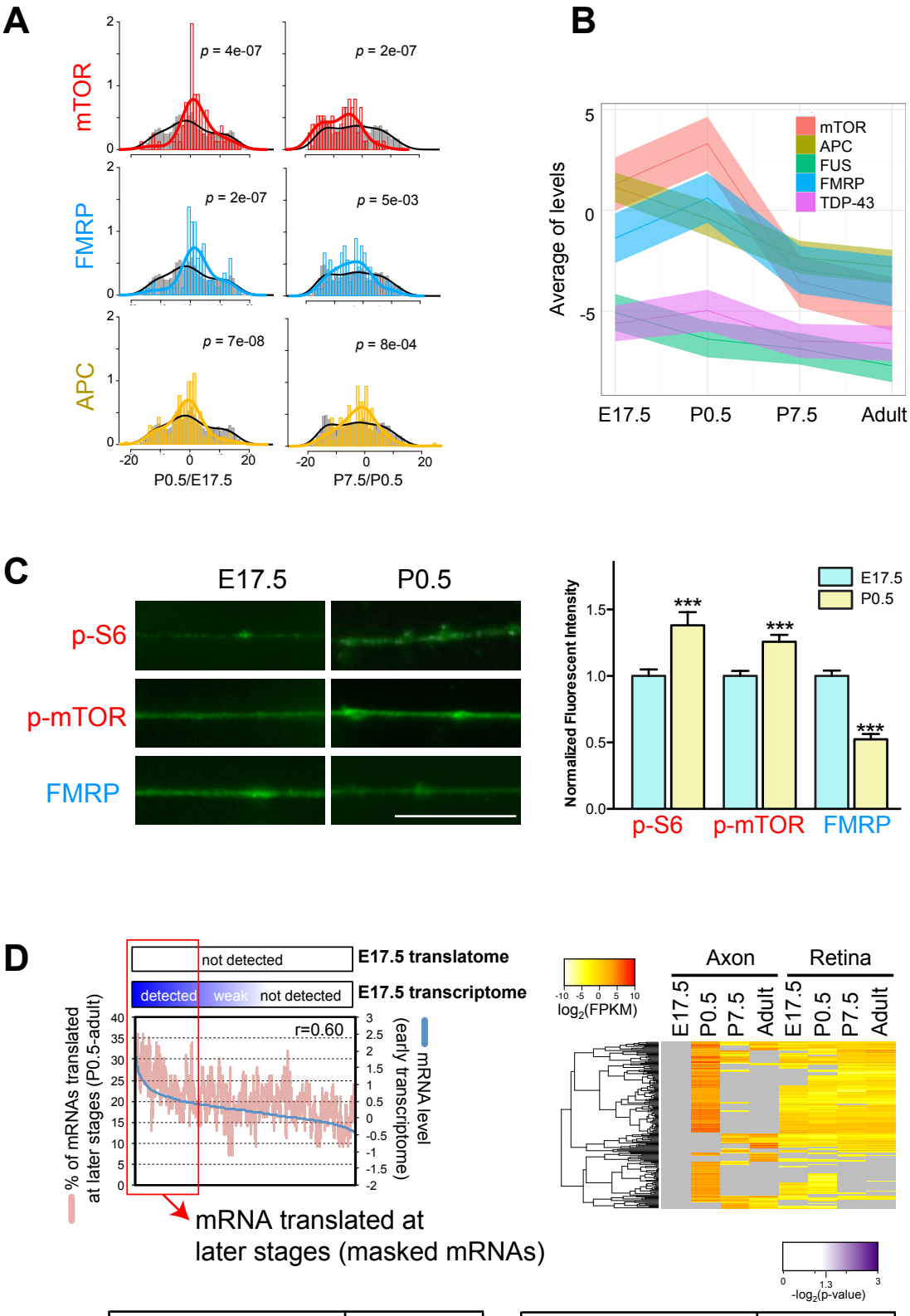

Upstream regulator	Unmasked stage		
	P0.5	P7.5	Adult
miR-3064-5p (w/seed CUGGCUG)			
miR-138-5p (w/seed GCUGGUG)			
miR-491-5p (w/seed GUGGGGA)			

Pathways	Unmasked stage		
	P0.5	P7.5	Adult
Dopamine Receptor Signaling			
Wnt/β-catenin Signaling			
Oleate Biosynthesis			

Figure 6

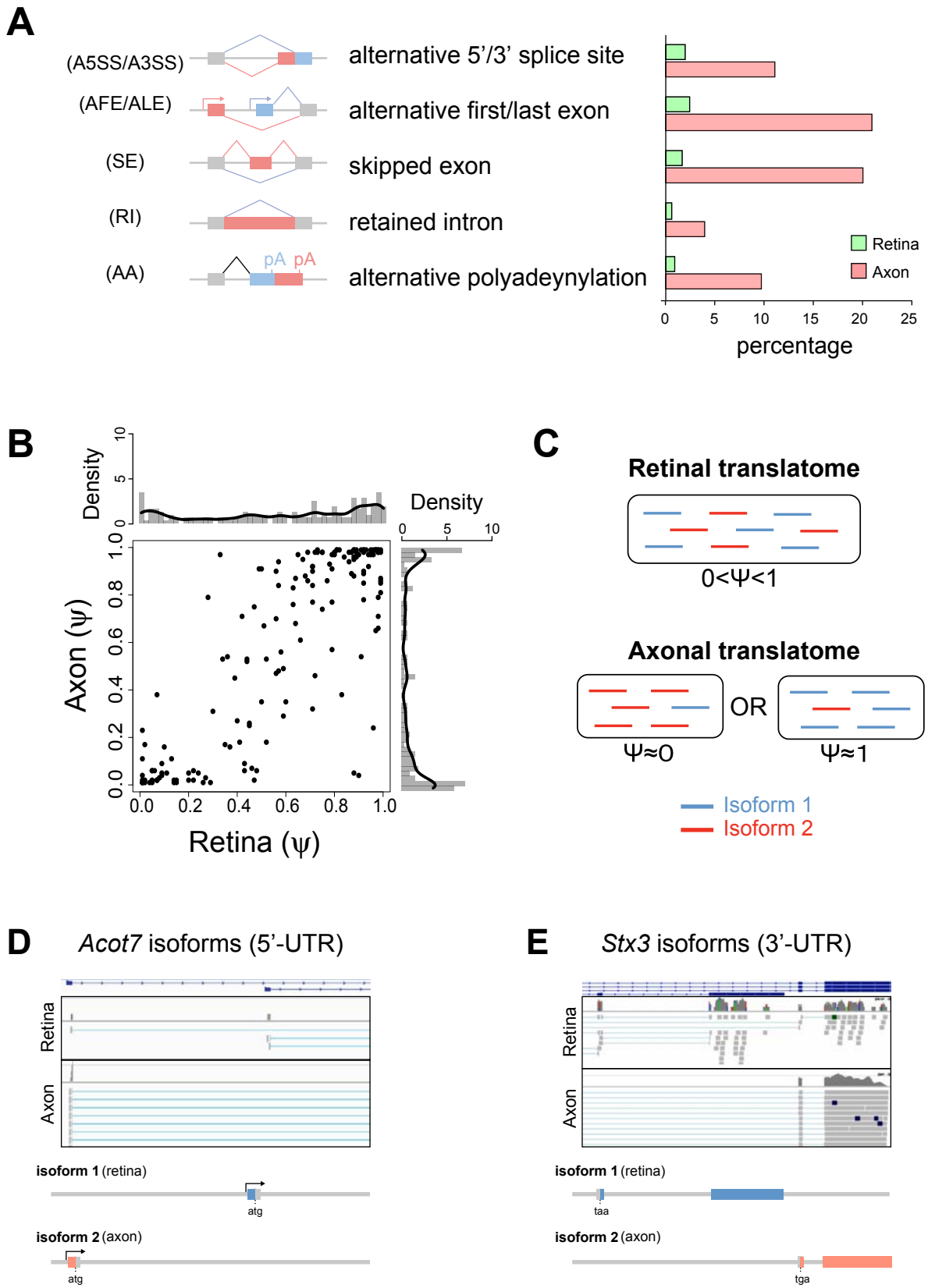

Figure 7

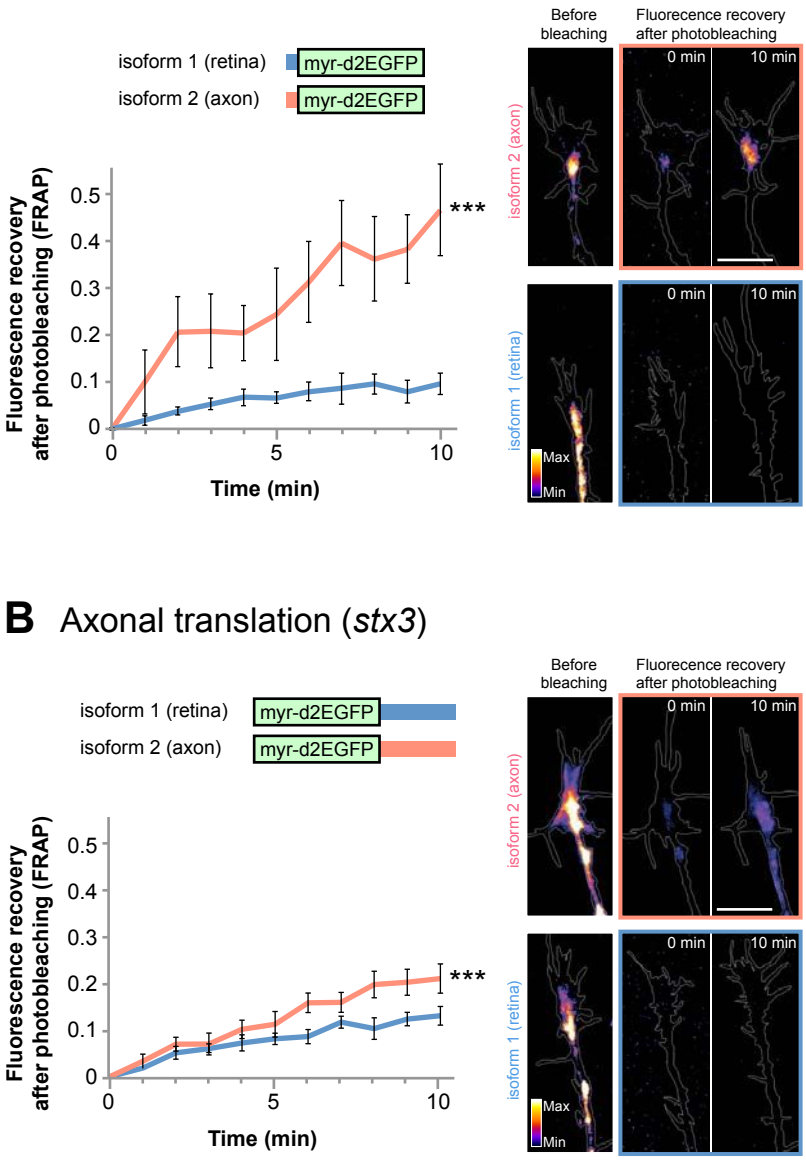

SUPPLEMENTAL INFORMATION

Dynamic axonal translation in developing and mature visual circuits

Toshiaki Shigeoka[1,4], Hosung Jung[2,4,5], Jane Jung[2], Benita Turner-Bridger[1], Jiyeon Ohk[2], Julie Qiaojin Lin[1], Paul S. Amieux[3], Christine E. Holt[1,5]

[1]Department of Physiology, Development and Neuroscience, University of Cambridge, Downing Street, Cambridge, CB2 3DY, United Kingdom.

[2]Department of Anatomy, Brain Research Institute, and Brain Korea 21 PLUS Project for Medical Science, Yonsei University College of Medicine, Seoul, 03722, Republic of Korea.

[3]Bastyr University Research Institute, Bastyr University, Kenmore, WA 98028, USA.

[4]Co-first author

[5]Co-senior author

*Correspondence should be addressed to H.J. (hosungjung@yonsei.ac.kr) or C.E.H. (ceh33@cam.ac.uk)

EXTENDED EXPERIMENTAL PROCEDURES

Animals

RiboTag and Pax6-alpha-Cre mice were kind gifts from Dr Paul Amieux (University of Washington) and Dr Peter Gruss (Max Planck Institute), respectively. A homozygote RiboTag female mouse was mated with a Pax6-alpha-Cre male, to produce Cre-positive and Cre-negative mice in a single litter. Cre-negative embryos or pups were used as negative controls for TRAP. Rosa26-StopLox-LacZ and Rosa26-StopLox-TauLacZ were kindly provided by Dr Jin-Woong Bok (Yonsei University) and Dr Soochul Park (Sookmyung Woman's University), respectively. All procedures were conducted under license in accordance with UK Home office guidelines and under the Guidelines for the Care and Use of Laboratory Animals of Yonsei University College of Medicine.

Monitoring of Cre-recombinase activity in Pax6-alpha-Cre mice

As even slightly leaky expression of the HA-tagged ribosome in any SC-resident cells would lead to misidentification of axonally translating mRNAs, we needed to confirm that no resident cells in the SC express Cre. We took two independent approaches. In the first, we used two Cre-responsive reporter mice: one that labels the cell bodies of Cre-expressing cells and their progeny (Rosa26-StopLox-LacZ) and the other that labels the axons of these cells (Rosa26-StopLox-TauLacZ). In accordance with the previous reports (Marquardt et al., 2001), LacZ-positive cell bodies were only observed in the neural retina but not in the SC (Fig. S1). Using the StopLox-TauLacZ reporter mouse to visualize retinal axons, we could see the SC is richly innervated by the axons originating from their Cre-positive cell bodies in the retina (Fig. S1). In the second approach, we crossed this mouse with RiboTag (Fig. 1C), and asked whether we could detect any trace of the recombined *RiboTag* allele (*HA-rpL22)* in the SC. If the SC contains any resident cells that have expressed Cre but escaped our

histological analysis, the nuclear DNA extracted from this tissue must contain the *HA-rpL22* allele, which we can detect using PCR-based assays (Fig. 1D). We detected no such signal in the SC dissected for TRAP (Figs. 1D and S1, red box). Therefore, both histological and molecular biological assays confirm that the only source of HA-tagged ribosomes in the SC is the RGC axons. Genotyping was performed by polymerase chain reaction (PCR) using the following primer pairs: for the Cre transgene, forward 5'- GCATTACCGGTCGATGCA ACGAGTG-3', and reverse 5'- GAACGCTAGAGCCTGTTTTGCACGTTC-3'; for the RiboTag allele, forward 5'-GGGAGGCTTGCTGGATATG-3, and reverse 5'- TTTCCAGACACAG-GCTAAGTACAC-3'; for detection of the recombined RiboTag allele (HA-rpL22), forward 5'-TTCTCTAGAAAGTATAGGAACTT-3', and reverse 5'-ACATCGTATGGG-TATAGATCC-3'. Cre-negative embryos or pups were used as negative controls for TRAP.

Quantitative reverse transcription-polymerase chain reaction (qRT-PCR)

cDNA was synthesized using an oligo-dT primer and SuperScript III reverse transcriptase (Invitrogen). The qPCR was performed using QuantiTect SYBR Green PCR Kit (Qiagen) on Light Cycler LC480 II (Roche). The levels were normalized by the total RNA amounts. The following primer pairs were used: for Glud1, forward 5'-GGGAGGTCATCGAAGGCTAC-3', and reverse 5'-AGCCAGTGCTTTTACTTCAT-CC-3'; for Mapt, forward 5'-TTCTGTCCTCGCCTTCT-GTC-3', and reverse 5'-CCTTCTTGGTCTTGGAGCAG-3'; for Rps5, forward 5'-TCAAGCTCTTTGGGAAAT-GG-3', and reverse 5'-GGGCAGGTACTTGGCATACT-3'; for Tsc2, forward 5'-TAGGGCTCCTGGTCATCCTT-3', and reverse 5'-GTGCT-TGTAATGGAGCTGGA-3'; for Cfl1, forward 5'-TCTGTCTCCCTTTCGTTTCC-3', and reverse 5'-GCCTTCTTGCGTTTCTTCAC - 3', for Aldoa, forward 5'-TTAGTCCTTTCGCCTA-CCCA-3', and reverse 5'-AGCTCCTTCTTCTGCTCCG-3'; for Atp5b, forward 5'-CACAATGCAGGAAAGGATCA-3', and reverse 5'-GGGTCAGTCAGG-TCATCAGC-

3'; for Basp, forward 5'-ACAAAGACAAGAAGGCCGAA-3', and reverse 5'-CTCTCCTTGACCTCGGTGG-3'; and for Cend1, forward 5'-CCTGAGCACT-CCTCGGTATC-3', and reverse 5'-AGACCACAGTGGCTCAGGAC-3'.

Histological analysis

Mouse embryos were fixed by immersion in 4% paraformaldehyde in PBS. Adult mice were transcardially perfused with the same fixative, and entire eyes and brains were dissected out and post-fixed. For X-gal staining, brains and retinae were dissected out, washed in ice-cold PBS and fixed for 1 hour in 1% formaldehyde, 0.2% glutaraldehyde, 2mM $MgCl_2$, 5mM EGTA, 0.02% NP-40 in PBS [pH7.5]) at 4°C on a shaker. The dissected tissues were rinsed three times for 20 min each in PBS and stained with X-gal staining solution (1mg/ml X-gal diluted in DMF, 0.01% Sodium deoxycholate, 0.02% NP-40, 5 mM potassium ferricyanide, 2 mM $MgCl_2$ in PBS) between 3 to 48 hours at 37°C in the dark. After washing with PBS, the tissues were post-fixed in 4% paraformaldehyde in PBS for 30 min at 4°C. For immunohistochemistry, tissues were saturated in 30% sucrose, embedded in OCT, frozen on dry ice, sectioned at 12 µm by using a cryostat (Leica CM3050S), and then visualized using an anti-HA antibody (Abcam ab9110) and a secondary antibody conjugated to Alexa Fluor 488 (Life technologies). For immuno-gold electron microscopy, tissues were fixed in 4% paraformaldehyde in 0.1M HEPES (pH 7.4), and the HA-tagged ribosomes were visualized by the same anti-HA antibody and IgG conjugated with gold (10nm-15nm) at the Cambridge Advanced Imaging Centre (University of Cambridge, UK). Specific labeling was evident as ultrastructurally identifiable ribosomes were labeled by multiple gold particles (Fig. 1F, purple arrows). We did, however, occasionally observe scattered gold particles in the Cre-negative tissue (Fig. 1G, white arrow), but these were never clustered as seen in the Cre-positive group. Therefore, we considered only two or more gold particles in close

proximity (within 50 nm between particles) as specific labeling of HA-positive ribosomes.

Axon-Translating Ribosome Affinity Purification (TRAP)

Tissue samples were dissected and snap-frozen in liquid nitrogen and genotyped. Whole eyes were used as the cell body group and the superior colliculus, where retinal axons terminate, were used as the axon terminal group. Tissues from cre-positive and negative were pooled for TRAP (three eyes and superior colliculi for one group). Tissues were homogenized in lysis buffer (20mM HEPES-KOH, 5mM $MgCl_2$, 150mM KCl, 1mM DTT, SUPERase In, and Complete EDTA-free Protease Inhibitor Cocktail) in the presence of cycloheximide (to stop translational elongation and to lock translating ribosomes on the mRNA) and rapamycin (to prevent new translational initiation during immunoprecipitation), and post-mitochondrial fractions were collected. We optimized the TRAP protocol before performing axon-TRAP. First, we found the polyclonal HA antibody (9110, Abcam) is superior to the one used in the original RiboTag study (HA11, Covance) (Sanz et al., 2009). Although the two antibodies were similarly effective in precipitating HA-rpL22, the polyclonal antibody (Abcam ab9110) co-purified much more 80S ribosomes (Fig. 2A). We estimated that approximately 40% of HA-tagged translating ribosomes could be purified this way, as the amount of TRAPed 80S ribosomes (i.e. co-immunoprecipitated rpS3a, a 40S ribosomal protein) was approximately 10% of the input (i.e. rpS3a in total input) (Fig. 2A). This estimation is based on the findings that (1) roughly 50% of retinal cells express HA-tagged rpL22 (i.e. 50% cells do not express tagged ribosomes), and that (2) these cells express rpL22 from one wildtype allele and one recombined HA-rpL22 allele (*i.e*. 50% of rpL22 is labeled with HA in Cre-positive cells) ([total 80S] = [HA-80S] x (1/50%) x (1/50%) = [TRAPed HA-80S] x (1/10%). Therefore, [TRAPed HA-80S] = (4/10) x [HA-80S]) (Fig. 2A). We found that the indirect immunoprecipitation protocol, which allows the antibody to bind the antigen before the purification of the

antigen-antibody complexes, was more specific than the direct protocol, which utilizes the antibody pre-conjugated to Protein G-magnetic beads. We think that nonspecific binding of mRNAs to Protein G-magnetic beads was reduced in the indirect protocol, as the tissue lysate was pre-cleared with unconjugated Protein G-magnetic beads. Pre-cleared ribosome-mRNA complexes were immunoprecipitated by an anti-HA antibody and Dynabeads Protein G (Life Technologies 10004D). Total RNA was extracted from the ribosome-mRNA complexes using an RNeasy mini kit (Qiagen) followed by in-column DNase treatment to remove genomic DNA contamination. The RNA samples were examined for quantity and quality using the Agilent Bioanalyzer 2100 (Agilent Technologies).

Amplification of cDNAs

The amount of axon-TRAPed mRNA was minute and had to be amplified (Fig. S2A). We used a method developed by Tang and colleagues for single cell transcriptomics (Tang et al., 2009) with slight modification (Fig. S2A). First, TRAPed RNAs were treated with DNase I to eliminate genomic DNA contamination and then mRNAs were reverse-transcribed with oligo(dT) primer with a linker. After second strand synthesis with another linker, the double-strand cDNAs were amplified by ten rounds of PCR and visualized by agarose gel electrophoresis (Fig. 2B). The specificity of TRAP was evident because it was dependent on Cre. As expected, the amount of TRAPed mRNAs was lower in the SC (mRNAs from RGC axons) than in the eye (mRNAs from the cell body and proximal neurites), and therefore was further amplified by five additional rounds of PCR. Although axon-TRAP was clearly dependent on Cre and therefore specific, increasing PCR cycles led to an increased background (i.e. amplified cDNAs from the Cre-negative SC). We reasoned that the amplified DNAs in the Cre-negative SC would reflect the relative abundance of mRNAs in the SC. We sequenced these mRNAs and used the data as a negative control for bioinformatics analysis of axon-TRAPed mRNAs (Fig. 2B). Amplified

cDNAs were subjected to paired-end 100 or 90 bp sequencing on the Illumina HiSeq2000.

For the *in vitro* ribosome run-off experiment, eyes or superior colliculi were homogenized by the 400 µl lysis buffer without cycloheximide, and then 200 µl of rabbit reticulocyte lysate (Promega) and 8 µl of Harringtonine (100 ug /ml) and 4 µl of 4E1RCat (5 mM) were added to the 188 µl lysate, followed by 37 °C incubation for 30 min. To stop the *in vitro* translation elongation, 800 µl of ice-cold lysis buffer with cycloheximide was added, followed by immunoprecipitation with the anti-HA antibody. The purified RNAs were subjected to RNA sequencing on the Illumina NextSeq 500. To reflect the difference in amount of amplified cDNAs between the samples with and without run-off translation on the sequencing depth, we first measured the amount of cDNA by both Tapestation DNA and by Qubit. We then adjusted the ratio between the amounts of input libraries for multiplex sequencing using the ratio of cDNA amount between the two samples. All RNA-seq data are deposited in Gene Expression Omnibus (GEO) datasets under accession number GSE79352.

Mapping of sequence reads and normalization of read counts

The sequence reads were mapped to the mouse genome (mm10) using TopHat 2 version 2.0.12 (Kim et al., 2013) with default settings, except for the "--read- realign-edit-dist 0" option. This option was chosen to reduce mapping to pseudogenes. Although we detected a significant number of sequencing reads of the primer dimers in several samples, which are probably caused by the matching problem between our primers and Illumina primers, because there is no biological reason that these dimers bias the relative abundance of sequence reads of endogenous mRNAs, we analyzed all sequence reads that can be mapped to the mouse genome sequence by TopHat 2. Transcript assembly and estimation of FPKM (Fragments Per Kilobase of

transcript per Million fragments sequenced) values were performed using Cufflinks version 2.2.1 (Trapnell et al., 2010). Read counts for each gene were determined using HTSeq version 0.6.1p1 (http://www- huber.embl.de/users/anders/HTSeq/). For the analysis of run-off samples, we used the read counts for all DEGs (adult) detected either in the run-off positive or negative sample.

Differential gene expression analysis and Gene Ontology based enrichment analysis

For the identification of translated mRNAs in RGC axons, we applied the differential gene expression analysis on read count data between two biological replicates of Cre-positive and Cre-negative samples using NOISeq (Tarazona et al., 2011) in default conditions with probability threshold 0.7. Although this approach has a risk of filtering out actively translating mRNAs if the same mRNAs exist in high abundance in SC-resident cells and are proportionately represented in the negative control, we thought that it would be appropriate to take a conservative approach when analyzing mRNAs identified by highly sensitive RNA-seq from samples with potentially low signal-to-noise ratio. DEG analysis identified a subset of Cre-dependent mRNAs (Fig. 2D, right panel, red dots) (Table S1). In some cases, genes that passed our filtering criteria and were identified as DEGs in one stage failed the same test in other stages (Fig. 2D, orange), because their abundance in the negative control varied depending on the stage. Most of these mRNAs, however, were found in the axon-TRAPed mRNAs at all stages tested, suggesting that these genes became false negatives in other stages. Therefore, when we analyzed the developmental change in translation levels, we used the FPKM (fragments per kilobase of transcript per million mapped reads) values of all four stages for genes that have passed the DEG test in at least one stage (Union of DEGs) (Fig. 2D, orange and peach).

To perform a GO-based analysis for neuronal functions (Figs. 4A and S4A), we selected 455 neuron-related GO terms (Table S2) using the following criteria: all offspring GO terms (249 terms) of 'Neuron development (GO:0048666)', which contain GO terms related to neuron/axon development, and all offspring GO terms (206 terms) of "Synaptic transmission (GO:0007268)", which contain GO terms related to neurotransmission. The offspring GO terms were identified using the GOBPOFFSPRING function of GO.db, an R package (Table S2). The enrichment analysis for gene ontology was carried out with DAVID and topGO version 2.18. (Alexa et al., 2006) on R version 3.1.2. The result for all analyzed GO terms (biological process) is represented in Table S3. For Kyoto Encyclopedia of Genes and Genomes (KEGG) analysis, we used all 2576 axonally translated genes and calculated p values and fold enrichments using DAVID (Fig. 4A, lower panel). The numbers of GO terms associated with retinal and axonal translatome were analysed using ClueGO (Bindea et al., 2009). Statistically significant enrichment is annotated by a solid box outline.

Ingenuity Pathway Analysis

Ingenuity Pathway Analysis (Qiagen) for canonical pathways (Fig. 5A) was performed according to the manufacturer's instructions. For quantitative analysis of stage-dependent axonal translation of each mRNA, we calculated the ratio in read counts of each mRNA from one stage to the next. Then we performed Ingenuity Pathway Analysis (IPA) for upstream regulators, which mainly utilizes published results of gene knockdown or knockout studies. For example, if the protein product of a gene decreases when a specific translational regulator is knocked out, the gene would be described as "positively regulated" by the translational regulator (and vice versa) (Fig. 5B).

Analysis of target mRNAs in the mTOR pathway and RNA binding proteins

We analyzed the known binding targets of RBPs using the results of previous studies on FMRP, TDP-43, FUS and APC. In addition, we carried out the same analysis on the targets of mTORC1 to confirm the result of IPA analysis. If any of these molecules regulate stage-specific translation in the axon, their target mRNAs would show coordinate changes in translation. We used the gene sets that were identified in previous studies (Colombrita et al., 2012; Darnell et al., 2011; Preitner et al., 2014; Thoreen et al., 2012). We analyzed mTOR targets that are described in the previous report (Thoreen et al., 2012) with a threshold of log2 (Torin1/Vehicle) < -1, FMRP targets (Darnell et al., 2011) with a threshold of rank (based upon chi-square score) < 100 and all of the APC targets (Preitner et al., 2014), TDP-43 targets and FUS targets identified(Colombrita et al., 2012). In the FPKM ratio analysis for consecutive developmental stages, we used all genes that were detected in RNA-seq in order to avoid any bias caused by differential gene expression analysis. Principle component analysis (PCA) was performed on normalized read counts of all samples to compare gene expression in 12 different conditions by using the “prcomp” function in the R Software package (version 2.13.0). Data were plotted using the first two PCs which explained up to 73.2% of the total variance: 66.1% explained by PC1; and 7.1% by PC2.

Analysis of mRNA isoforms

Alternative isoforms were analyzed on mapped reads from the P0.5 sample using MISO. Before this analysis, the mean and the standard deviation of the insert length and the total number of mapped read pairs were computed using the “pe_utils” utilities (Retina: mean=177.8, sdev=9.7, dispersion=0.7, num_pairs=3262858, Axon: mean=178.3, sdev=13.5, dispersion=1.0, num_pairs=2535309, Cre_negative axon: mean=179.6, sdev=9.2, dispersion=0.7, num_pairs=3235484). We used Mouse genome (mm10) alternative events version 1.0 (Wang et al., 2008) to perform “exon-centric” analyses. We counted and analyzed only the events in which both splicing

variants are detected both in axon and in cell body (the events of “0 < Ψ <1" both in axon and in cell body). For the discovery of novel splice variants, we performed reference-independent transcript reconstruction using Cufflinks version 2.2.1 (Trapnell et al., 2010) and compared the sequences of reconstructed transcripts with the UCSC Genes transcript annotations by using the Cuffcompare program from the Cufflinks package. For the identification of circular RNAs, we first extracted the fusion transcripts from the unmapped sequence reads by using TopHat-fusion (Kim and Salzberg, 2011) (TopHat 2.0.12, parameters:--fusion-search --keep-fasta-order --bowtie1 --no-coverage-search), and then identified junction reads from back spliced exons using CIRCexplorer-1.1.1(Zhang et al., 2014). Mapped sequence reads are visualized using the Integrative Genomics Viewer (IGV) version 2.3.46 (Robinson et al., 2011).

Identification of regulatory motifs in RNA

De novo motif analysis was performed using HOMER version 3.0 (Heinz et al., 2010) with custom FASTA files. For the finding of motifs in UTRs, we used the UTR sequences of genes whose levels were higher in the axon than in the retina (axon / retina > 100, Fig. 3A) in P0.5 translatomes. For finding of motifs in axon-enriched alternative exons, detection of differential exon usage was performed using DEXseq version 1.10.8 (Anders et al., 2012) on R version 3.1.0, and exons were selected with a Benjamini–Hochberg adjusted p-value cut-off of < 0.1 (Benjamini and Hochberg, 1995). To validate these motifs, we extracted the genes that contain these motifs allowing 0-1 mismatch and then compared the translation levels between axon and retina. Sequences of UTRs were retrieved from Ensemble BioMart (Kinsella et al., 2011). Motif containing genes were identified using the Biostrings package on R version 3.1.2.

Immunofluorescence

Mouse RGC axons were cultured as previously described (Zivraj et al., 2010). The cultures were fixed in 2% (vol/vol) paraformaldehyde/7.5% (wt/vol) sucrose, permeabilized with 0.1% Saponin (Sigma) and blocked in 5% goat serum, then labeled with primary antibodies overnight and Alexa Fluor 488 secondary antibodies (1:1000, Life Technologies), and mounted in FluorSave (Calbiochem). Randomly selected isolated axons were imaged with a Plan Apo 60X oil objective on a Nikon Eclipse TE2000-U inverted fluorescent microscope with a Hamamatsu ORCA-ER CCD camera. Exposure time was kept constant and below greyscale pixel saturation. For quantitation of fluorescence intensity, the outline of the axon segments with similar lengths was traced on the phase image using Volocity software (PerkinElmer), and then superimposed on the fluorescent image. The software calculated the fluorescent intensity within the axon segment, giving a measurement of pixel intensity per unit area. The axon outline was then placed in an adjacent area clear of cellular material to record the background fluorescent intensity. This reading was subtracted from the axon reading, yielding the background-corrected intensity. Each reading was normalized to the mean fluorescent intensity of E17.5 axons in the same group. The fluorescent intensities of between 50 to 100 axon segments per sample group were collected. The following antibodies were used: anti-mTOR (phospho S2448) antibody (Abcam 109268), anti-FMRP antibody (Abcam 17722), and anti-RPS6 (phospho S235 + S236) antibody (Abcam 12864).

Fluorescence recovery after photobleaching (FRAP)

Motif sequences were cloned into a plasmid containing the coding sequence of membrane-targeted, destabilized EGFP (myr-d2EGFP) (Aakalu et al., 2001) between NotI-XhoI sites (for 3'-UTR and alternative exon) or NheI-BamHI sites (for 5'-UTR). Motif sequences are in Table S3. The reporter plasmids were expressed in the retina by targeted electroporation into *Xenopus laevis* embryos, and fluorescence was imaged in cultured retinal ganglion cell axons as previously described (Leung et

al., 2006), except that 1% fetal bovine serum was added to the medium. In experiments to confirm translation-dependency of FRAP, the translation inhibitor anisomycin (40 μM) was added 30 min prior to imaging. FRAP experiments were performed on an Olympus IX81 inverted microscope equipped with a PerkinElmer Spinning Disk UltraVIEW VoX and a 60x (NA, 1.30) Olympus silicone oil immersion objective. Images were acquired with an ORCA-Flash4.0 V2 CMOS camera (Hamamatsu) using Volocity software (PerkinElmer).

Photobleaching was performed using an UltraVIEW PhotoKinesis device (PerkinElmer). Regions of interest were manually defined so that growth cones and ≥20μm of the axon shaft were bleached (thus reducing likelihood of fluorescence recovery resulting from myr-d2EGFP diffusion from unbleached areas of the axon shaft). Photobleaching was performed at 50-85% laser power (488 nm laser line) with 20–30 bleach cycles. Time-lapse images were captured at 1 min intervals using a 488 nm laser line at 25% laser power for myr-d2EGFP and a 561 nm laser line (31 % laser power) for visualization of axons using a membrane-targeted mCherry-CAAX reporter, in addition to phase contrast. Exposure time for the 488 channel was adjusted to avoid pixel saturation and was typically between 50-200ms. Quantification of fluorescence intensity was performed using Volocity software (PerkinElmer). At each time point, the outline of the growth cone (ROI) was traced using the mCherry-CAAX reporter (561 channel) and phase contrast images. Mean gray values from the 488 channel were subsequently calculated as mean pixel intensity per unit area within the ROI. Subtracting the mean background pixel intensity per unit area from an equivalently sized ROI immediately adjacent to the growth cone normalised intensity values in the growth cone. Unhealthy axons exhibiting signs of photo-toxicity after FRAP (characterised by blebbing, growth cone collapse and/or retraction) were excluded from analysis. In addition, we only quantified growth cones of axons extending more than 100 μm from the eye explant

to reduce effects of somal diffusion. Relative fluorescent recovery (R) at each time point was calculated by the formula: $R_x = (I_x – I_{post}) / (I_{pre} – I_{post})$. Where, I_x = normalised fluorescent intensity of the growth cone ROI at time point 'x', I_{pre} = normalised fluorescent intensity before photobleaching and I_{post} = normalised fluorescent intensity immediately after photobleaching (t=0 mins).

Data were analysed using PRISM software (Graphpad). Significance was tested using a two-way ANOVA.

REFERENCES

Aakalu, G., Smith, W.B., Nguyen, N., Jiang, C., and Schuman, E.M. (2001). Dynamic visualization of local protein synthesis in hippocampal neurons. Neuron *30*, 489-502.

Anders, S., Reyes, A., and Huber, W. (2012). Detecting differential usage of exons from RNA-seq data. Genome research *22*, 2008-2017.

Benjamini, Y., and Hochberg, Y. (1995). Controlling the False Discovery Rate - a Practical and Powerful Approach to Multiple Testing. J Roy Stat Soc B Met *57*, 289-300.

Colombrita, C., Onesto, E., Megiorni, F., Pizzuti, A., Baralle, F.E., Buratti, E., Silani, V., and Ratti, A. (2012). TDP-43 and FUS RNA-binding proteins bind distinct sets of cytoplasmic messenger RNAs and differently regulate their post-transcriptional fate in motoneuron-like cells. J Biol Chem *287*, 15635-15647.

Darnell, J.C., Van Driesche, S.J., Zhang, C., Hung, K.Y., Mele, A., Fraser, C.E., Stone, E.F., Chen, C., Fak, J.J., Chi, S.W.*, et al.* (2011). FMRP stalls ribosomal translocation on mRNAs linked to synaptic function and autism. Cell *146*, 247-261.

Heinz, S., Benner, C., Spann, N., Bertolino, E., Lin, Y.C., Laslo, P., Cheng, J.X., Murre, C., Singh, H., and Glass, C.K. (2010). Simple combinations of lineage-determining transcription factors prime cis-regulatory elements required for macrophage and B cell identities. Molecular cell *38*, 576-589.

Kim, D., Pertea, G., Trapnell, C., Pimentel, H., Kelley, R., and Salzberg, S.L. (2013). TopHat2: accurate alignment of transcriptomes in the presence of insertions, deletions and gene fusions. Genome biology *14*, R36.

Kim, D., and Salzberg, S.L. (2011). TopHat-Fusion: an algorithm for discovery of novel fusion transcripts. Genome biology *12*, R72.

Kinsella, R.J., Kahari, A., Haider, S., Zamora, J., Proctor, G., Spudich, G., Almeida-King, J., Staines, D., Derwent, P., Kerhornou, A.*, et al.* (2011). Ensembl BioMarts: a hub for data retrieval across taxonomic space. Database : the journal of biological databases and curation *2011*, bar030.

Leung, K.M., van Horck, F.P., Lin, A.C., Allison, R., Standart, N., and Holt, C.E. (2006). Asymmetrical beta-actin mRNA translation in growth cones mediates attractive turning to netrin-1. Nat Neurosci *9*, 1247-1256.

Marquardt, T., Ashery-Padan, R., Andrejewski, N., Scardigli, R., Guillemot, F., and Gruss, P. (2001). Pax6 is required for the multipotent state of retinal progenitor cells. Cell *105*, 43-55.

Preitner, N., Quan, J., Nowakowski, D.W., Hancock, M.L., Shi, J., Tcherkezian, J., Young-Pearse, T.L., and Flanagan, J.G. (2014). APC is an RNA-binding protein, and its interactome provides a link to neural development and microtubule assembly. Cell *158*, 368-382.

Robinson, J.T., Thorvaldsdottir, H., Winckler, W., Guttman, M., Lander, E.S., Getz, G., and Mesirov, J.P. (2011). Integrative genomics viewer. Nature biotechnology *29*, 24-26.

Sanz, E., Yang, L., Su, T., Morris, D.R., McKnight, G.S., and Amieux, P.S. (2009). Cell-type-specific isolation of ribosome-associated mRNA from complex tissues. Proc Natl Acad Sci U S A *106*, 13939-13944.

Tang, F., Barbacioru, C., Wang, Y., Nordman, E., Lee, C., Xu, N., Wang, X., Bodeau, J., Tuch, B.B., Siddiqui, A.*, et al.* (2009). mRNA-Seq whole-transcriptome analysis of a single cell. Nat Methods *6*, 377-382.

Tarazona, S., Garcia-Alcalde, F., Dopazo, J., Ferrer, A., and Conesa, A. (2011). Differential expression in RNA-seq: a matter of depth. Genome research *21*, 2213-2223.

Thoreen, C.C., Chantranupong, L., Keys, H.R., Wang, T., Gray, N.S., and Sabatini, D.M. (2012). A unifying model for mTORC1-mediated regulation of mRNA translation. Nature *485*, 109-113.

Trapnell, C., Williams, B.A., Pertea, G., Mortazavi, A., Kwan, G., van Baren, M.J., Salzberg, S.L., Wold, B.J., and Pachter, L. (2010). Transcript assembly and quantification by RNA-Seq reveals unannotated transcripts and isoform switching during cell differentiation. Nature biotechnology *28*, 511-515.

Wang, E.T., Sandberg, R., Luo, S., Khrebtukova, I., Zhang, L., Mayr, C., Kingsmore, S.F., Schroth, G.P., and Burge, C.B. (2008). Alternative isoform regulation in human tissue transcriptomes. Nature *456*, 470-476.

Zhang, X.O., Wang, H.B., Zhang, Y., Lu, X., Chen, L.L., and Yang, L. (2014). Complementary sequence-mediated exon circularization. Cell *159*, 134-147.

Zivraj, K.H., Tung, Y.C., Piper, M., Gumy, L., Fawcett, J.W., Yeo, G.S., and Holt, C.E. (2010). Subcellular profiling reveals distinct and developmentally regulated repertoire of growth cone mRNAs. J Neurosci *30*, 15464-15478.

LEGENDS FOR SUPPLEMENTAL FIGURES AND TABLES

Figure S1. Specific labeling of retinal axons in Retinal RiboTag, Related to Figure 1 (A) Two Cre activity reporter mice were used in this study. The LacZ reporter labels the cell bodies of Cre-positive cells and their progeny, whereas the TauLacZ reporter labels both the cell bodies and axons. **(B)** X-gal staining of the retina, optic chiasm (OC) and superior colliculus (SC) in alpha-Cre; LacZ reporter gene double positive mice. Cre labels most peripheral neural retinal cells in both mice. No cells in the SC used for TRAP in this study express Cre as evidenced by the lack of X-gal stain in the LacZ reporter SC. Unlike the alpha-Cre; LacZ mice, alpha-Cre; TauLacZ mice show robust staining not only in the cell bodies but also the OC and the SC. The SC, which was used for axon-TRAP, is highly innervated by retinal axons.

Figure S2. Axon-TRAP, Related to Figure 2 (A) Bioanalyzer analysis of axon-TRAPed mRNA. Lower tables show the amounts of total RNAs and amplified cDNAs for each TRAPed sample. **(B)** Silver staining of axon-TRAPed protein complexes following SDS-PAGE. **(C)** Strategy for cDNA synthesis and amplification adopted from the study from Tang et al. (**D)** Ribosome run-off experiment. The amplified cDNAs from TRAPed mRNAs with or without run-off (P0.5 retina). **(E)** Retinal and axon-TRAP combined with ribosome run-off. **(F)** Scatterplots of $\log_2$ (FPKM) between Cre-positive (x axis) and Cre-negative axons (y axis).

Figure S3. Comparison between the axonal and the retinal translatome, Related to Figure 3 (A) The upper panel shows a heat map of hierarchical clustering on the normalized level of axonal and retinal translation of genes. Each row in the heat map corresponds to a single gene. The color of the heat map represents the log2 (FPKM value) for each gene (grey = not detected). The lower panel shows a heat map of a

correlation matrix. **(B)** Tables showing the ranking of most significantly enriched GO terms in axon-enriched mRNAs and retina-enriched mRNAs. Terms presented in Figure 3B are shown in red. **(C)** A heat map showing the enrichment of GO terms in the biological process (BP) category. The colors of the heat map represents the log2 value of the fold enrichment for each GO term value (red = enriched, blue = depleted, grey = not detected), and the numbers on the heat map are –log 10 (Fisher's exact p-value) for enrichment.

Figure S4. Gene set enrichment analysis describing the developmental changes of translated genes in RGC axons, Related to Figure 4 (A) The upper heat map displays the enrichment of GO terms or KEGG pathways for axonally translated genes. Each row in the heat map corresponds to a single GO term. Genes are clustered either by stage-specific expression ("stages") or hierarchical clustering (lower heat map) according to their developmental changes ("changes"). **(B)** Ingenuity pathway analysis (IPA) to identify canonical pathways associated with the axonal translatome. Each row represents a single pathway (blue, enriched). The right panel shows lists of pathways extracted from each cluster. **C)** A heatmap showing the $\log_2$ (read count) for adult samples with and without ribosome run-off. Each row in the heat map corresponds to a single gene.

Figure S5. Analysis of *trans*-acting elements that regulate the axonal translatome, Related to Figure 5 (A) Ingenuity pathway analysis (IPA) to identify upstream regulators associated with the axonal translatome**.** The abundance of each mRNA between two consecutive stages was represented as the ratio (ratio > 1 indicates increase in translation). The coordinate change in the translation ratios was calculated as the activation z-score. A positive z-score indicates that the translational regulator is expected to be activated. **(B)** Bar graph representing the fold change in levels of axonally translated genes. The mRNA levels in the axonal translatome were

quantified by qRT-PCR (normalized by TRAPed cDNA for each stage). **(C)** Density plots showing the distribution of changes in FPKM values for the axonal translatome during two consecutive developmental stages with p-values (Komogorov-Smirnov test). The values are calculated as follows: log2 (stage A(FPKM) / stage B (FPKM)). The distributions of target genes in pathways, which are indicated by colored lines, are overlapped with non-target genes represented by grey line. **(D)** A scatter plot of the Principal Component Analysis (PCA) based on normalized read counts in the axonal and retinal translatome from four different stages. Data were plotted using the first two Principal Components (PCs), which explained up to 73.2% of the total variance. **(E)** Relationship between transcript abundance of the genes in E17.5 transcriptome, which were detected in E17.5 axonal translatome, and probability of their translation at later stages (blue line, mRNA level in transcriptome; red line, moving averages of percentage of genes detected at any of three later stages over a window size of 100 genes; r, Pearson correlation coefficient). The right heatmap show mRNA abundance in the translatome (left) and enriched pathways (right).

Figure S6. Analysis for alternative isoforms and *cis*-acting elements, Related to Figure 6 (A-B) Sequence reads (grey bars) mapped on the genes, *sarm1* (A) and *clta* (B). The mapped reads are visualized by Integrative Genomics Viewer (IGV) **(C)** Sequence reads (grey bars) mapped on the *rhobtb3* (upper panel). Sanger sequencing of RT-PCR fragment of the *ankrd1* (lower panel).

Figure S7. *Cis*-regulatory elements for axonal translation, Related to Figure 7 **(A)** Lists of sequence motifs enriched in 5'UTRs, 3'UTRs and alternative exons of axon-enriched mRNAs / exons. **(B)** An example of axon-enriched motifs. The scatterplot compares the normalized mRNA levels (log2(FPKM)) between the axonal (y axis) and the retinal (x axis) translatome at stage P0.5 for genes with (red dots) and without (black dots) the motif. The density plot shows the distribution of log2

(axon (FPKM) / retina (FPKM)). **(C)** GO enrichment analysis for entire genome containing axon-specific sequence motifs (K: G or T; R: A or G; Y: C or T; M: A or C; R: A or G; and H A or C or T) and their relative efficiency in axonal mRNA translation measured by fluorescence recovery after photobleaching (FRAP) of motif-containing reporter constructs (myr-d2EGFP). Several axon-specific motifs were able to promote mRNA translation in the growth cone relative to a control myr-d2EGFP construct without a UTR. Statistical significance of FRAP compared to the no-UTR control was tested across all time-points (0-10mins) using a two-way ANOVA (from the top bar, n=16, 5, 5, 7, 8, 7, 3, 8, 8, 8, 5, 8, and 6, respectively). For representative purposes, the mean fluorescence recovery at 10 minutes post-photobleaching is shown. Error bars represent SEM. **p<0.01, and ***<p0.001 compared to no-UTR control.

Table S1. Axonally translating mRNAs, Related to Figure 3

Table S2. Neuron-related GO terms, Related to Figure 4

Table S3. GO term and motif analysis, Related to Figure 5

Figure S1

A. Cre activity reporter mice

alpha-Cre / Rosa26-**LacZ**
(labels cell body only)

alpha-Cre / Rosa26-**TauLacZ**
(labels cell body & axon)

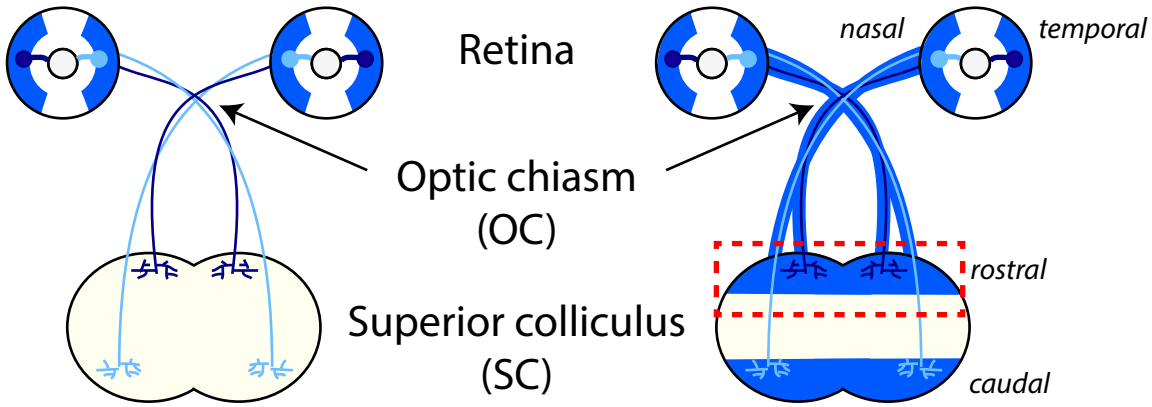

B. Labeled cells and axons in Retinal RiboTag

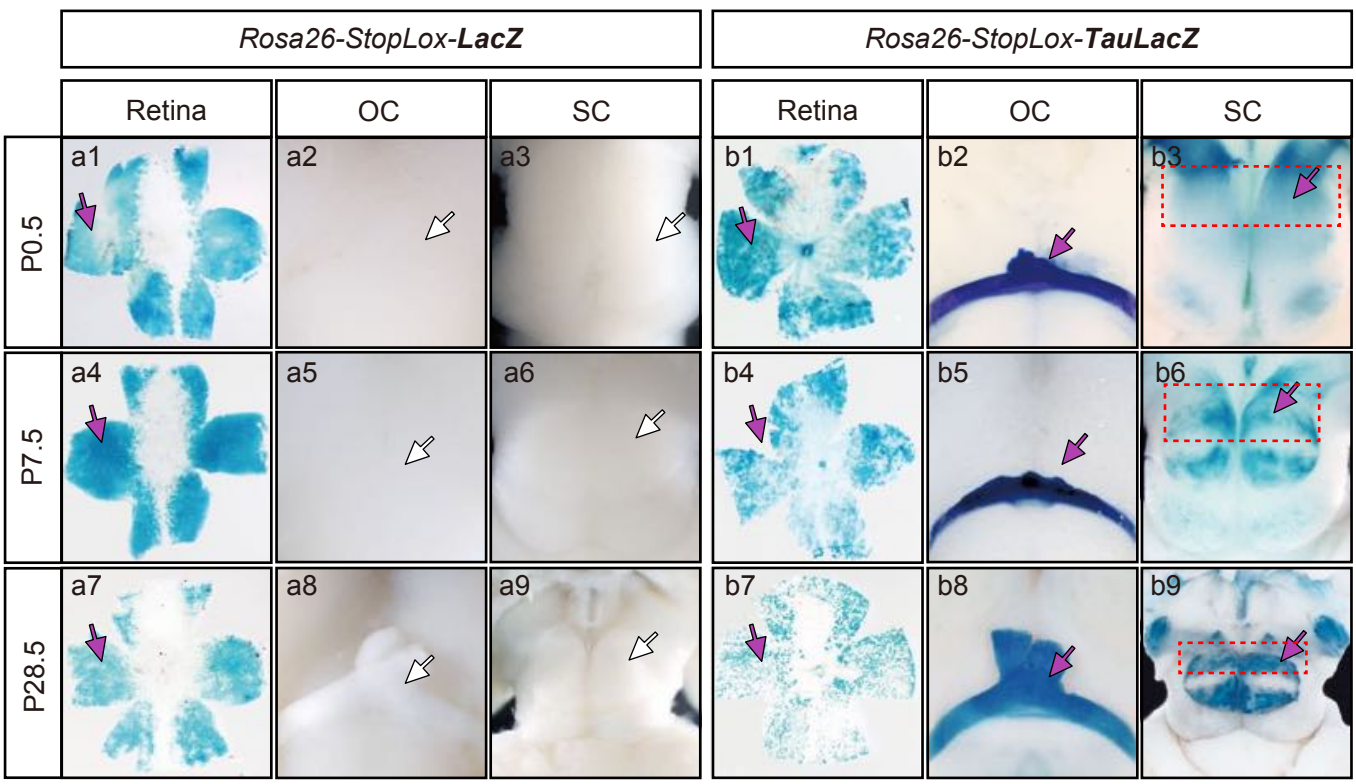

Figure S2

A. Bioanalyzer

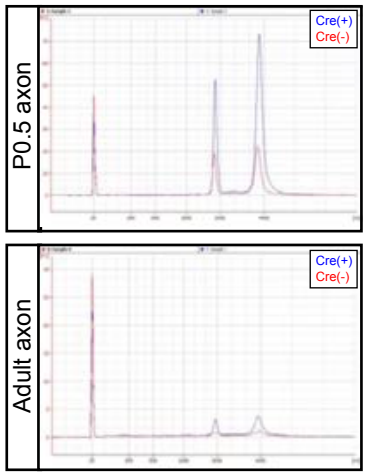

RNA (ng)	E17.5	P0.5	P7.5	Adult
Retina	26	18	34	20
Axon	3.2	2.8	3.1	0.4

cDNA (ng)	E17.5	P0.5	P7.5	Adult
Axon	1815	2475	590	275

(per animal)

C. cDNA synthesis

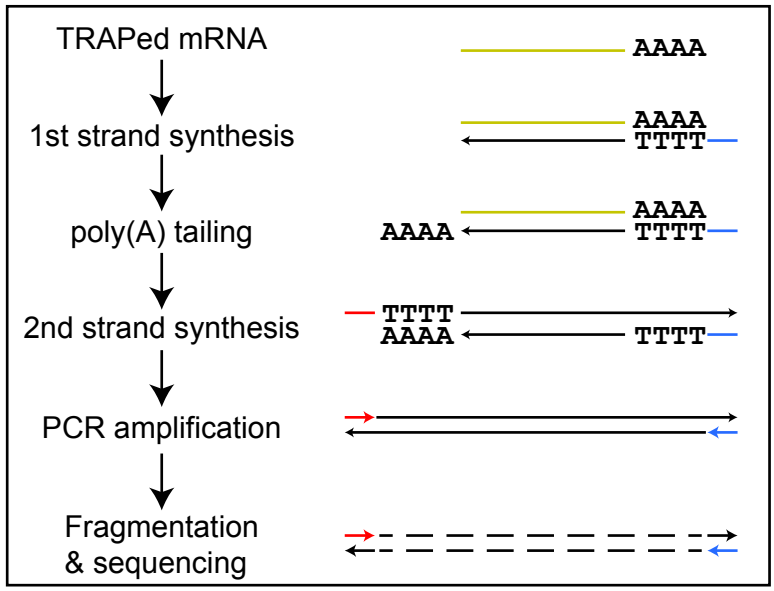

B. Silver staining

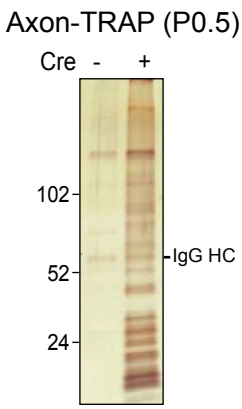

D. Ribosome run-off (P0.5)

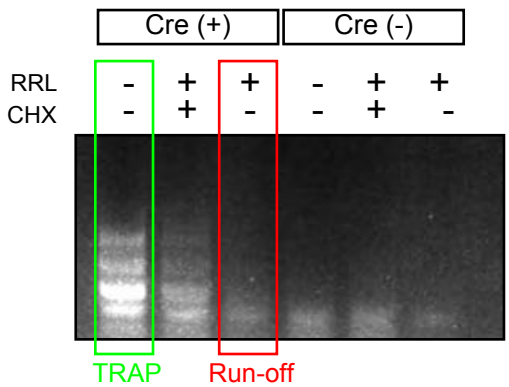

E. Run-off in axon

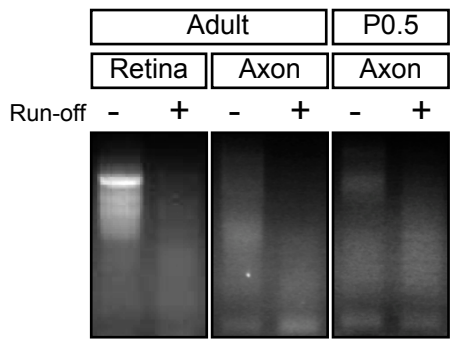

F. DEG analysis

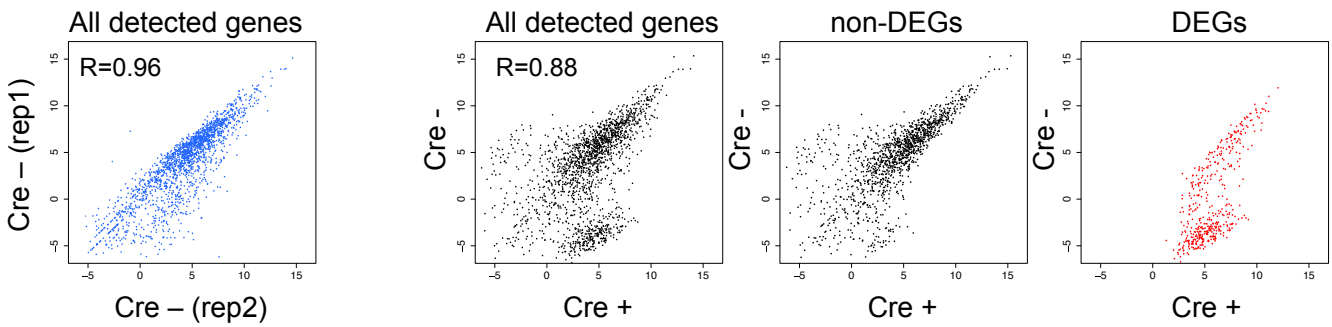

Figure S3

A

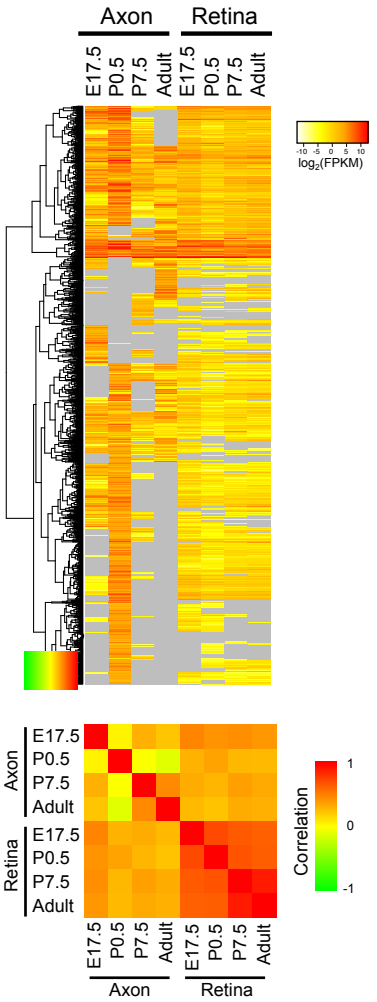

C

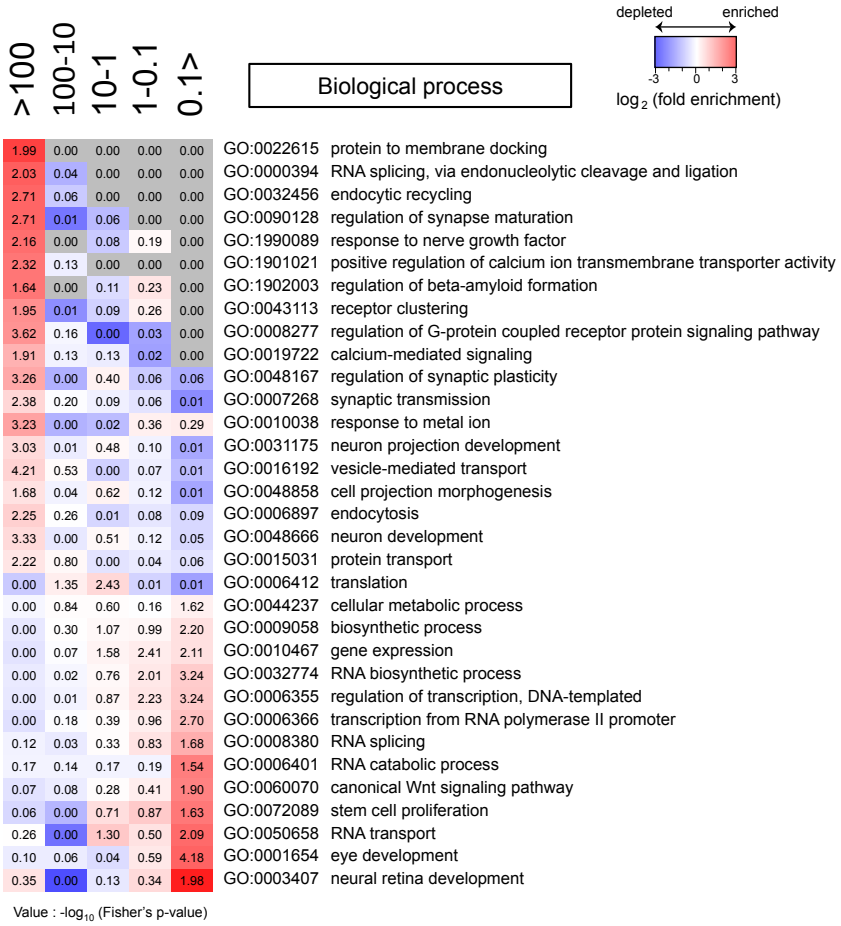

B

Axon-enriched mRNAs

Ranking	Term	*p*-value	Fold enrichment
1	cytoskeleton	8.E-10	1.9
2	vesicle	4.E-08	2.2
3	cytoplasmic vesicle	1.E-07	2.2
4	neuron projection	4.E-07	2.7
5	cytoplasmic membrane-bounded vesicle	2.E-06	2.2
6	synapse	2.E-06	2.4
7	cytoskeletal part	3.E-06	1.8
8	membrane-bounded vesicle	3.E-06	2.1
9	non-membrane-bounded organelle	4.E-06	1.4
10	intracellular non-membrane-bounded orga	4.E-06	1.4
11	perinuclear region of cytoplasm	6.E-06	2.8
12	actin cytoskeleton	2.E-05	2.6
13	endomembrane system	3.E-05	1.9
14	synapse part	4.E-05	2.5
15	microtubule cytoskeleton	4.E-05	1.9
16	Golgi apparatus	2.E-04	1.7
17	axon	2.E-04	3.1
18	microtubule	3.E-04	2.2

Retina-enriched mRNAs

Ranking	Term	*p*-value	Fold enrichment
1	intracellular organelle lumen	2.E-03	2.2
2	organelle lumen	2.E-03	2.2
3	spliceosome	3.E-03	6.2
4	nuclear lumen	3.E-03	2.3
5	membrane-enclosed lumen	3.E-03	2.1
6	nucleoplasm	6.E-03	2.6
7	ribonucleoprotein complex	9.E-03	2.8
8	nucleoplasm part	2.E-02	2.5
9	endoplasmic reticulum	3.E-02	2.0
10	nucleolus	3.E-02	2.9
11	endoplasmic reticulum part	3.E-02	3.3
12	centromeric heterochromatin	5.E-02	36.8
13	endomembrane system	5.E-02	2.2
14	chromosome, centromeric region	5.E-02	4.6
15	chromosome	7.E-02	2.4
16	non-membrane-bounded organelle	9.E-02	1.4
17	intracellular non-membrane-bounded orga	9.E-02	1.4
18	Golgi apparatus part	1.E-01	2.8

Figure S4

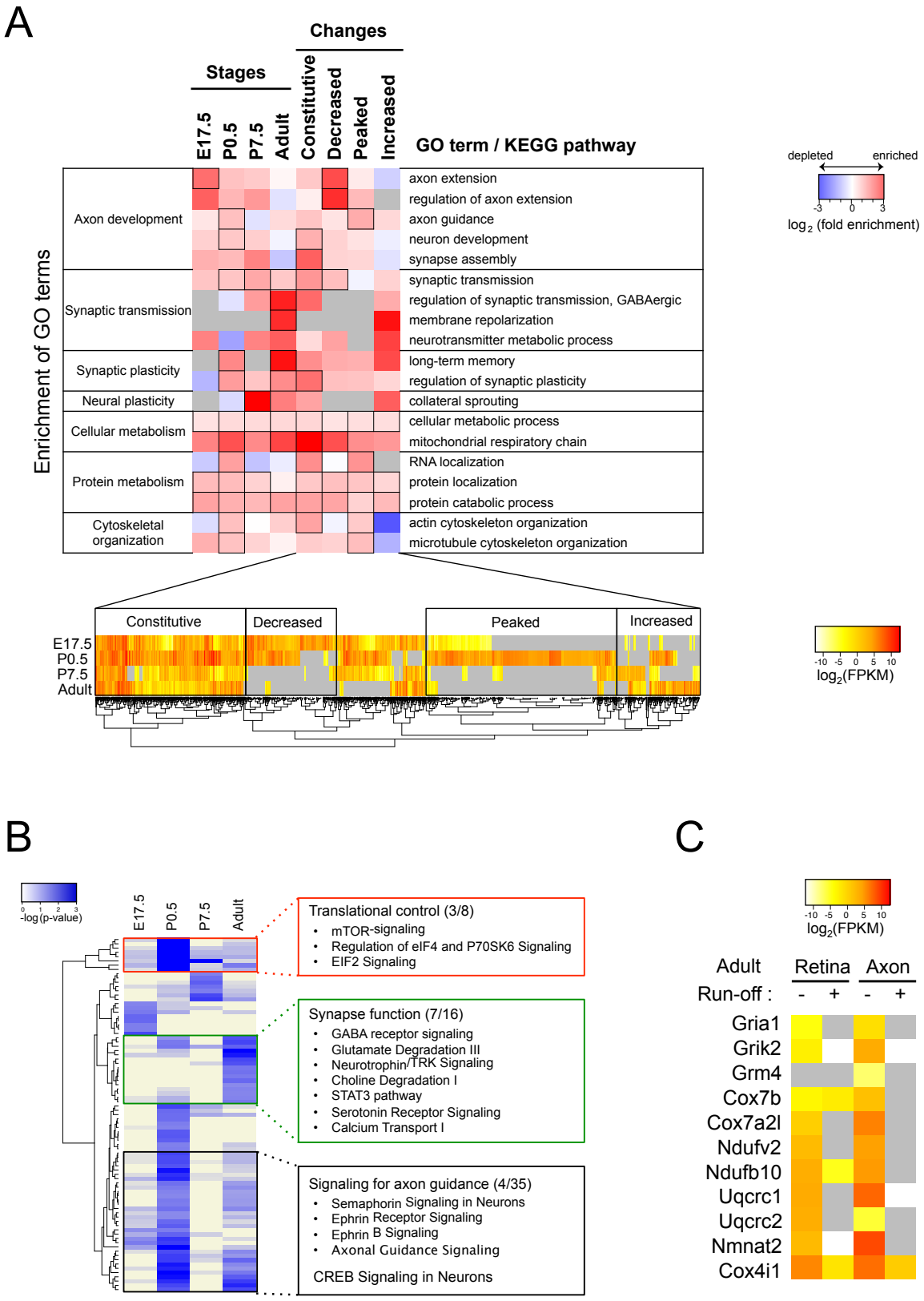

Figure S5

A

Upstream regulators	z-score to P0.5	z-score to P7.5	z-score to Adult	Type	Target mRNAs
mTOR	1.86			kinase	ACACA,ATG12,CACTIN,CASP3,CASP9,CCND1,CDKN1A,COX4I1,CS,ENO1,FAF1,FASN,FKBP1A,FN1,FOXP3,GLUD1,HADHA,INHA,MADD,MAPT,MDM2,NFKBIL1,PIP5K1C,PPARGC1B,PPP2CA,RBM5,RXRB,SMPD1,TCF4,TSC2
FMR1	0.08	2.49	0.35	RNA-binding protein	AGAP1,ALDOA,Ap2b1,APP,ATPIF1,BASP1,CEND1,CFL1,CTNNB1,ENO1,RAB3A,RPSA,SYP,TSC2,UQCRQ
miR-1	-1.74	1.37	2.22	microRNA	ANXA2,ATP6V0A1,CASP3,CCND2,FN1,HSPD1,IGF1R,LASP1,MKL1,MTX1,PAX7,TAGLN2

B

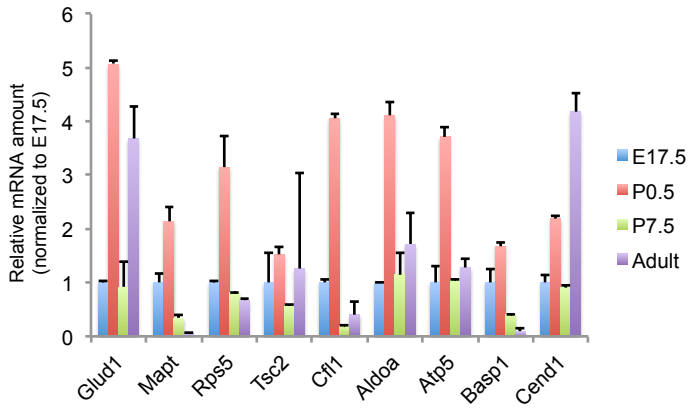

C

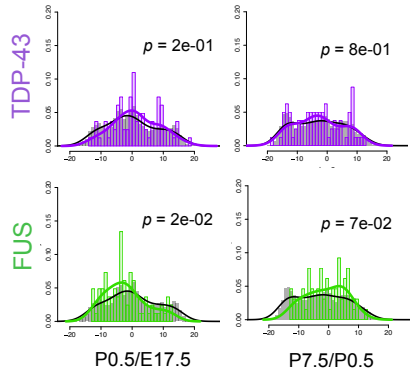

D

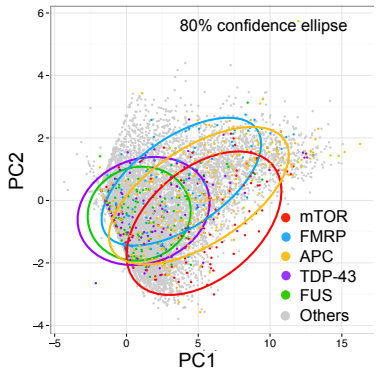

E

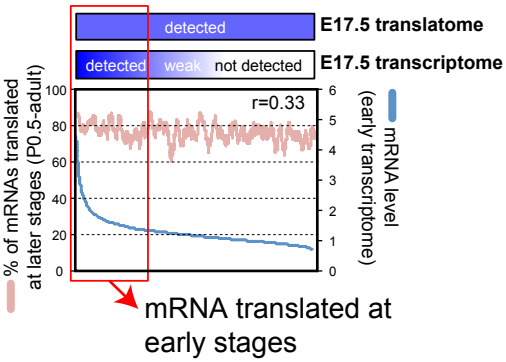

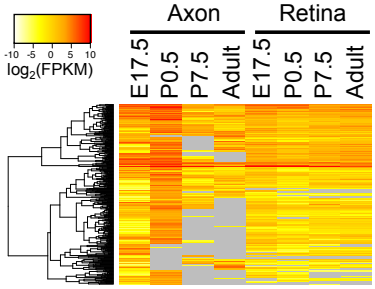

Pathway (E17 transcriptome)	Translating stage E17.5	P0.5	P7.5	Adult
Oxidative Phosphorylation	12.6	12.5	8.35	11
Mitochondrial Dysfunction	11.7	10.9	7.95	8.34
EIF2 Signaling	7.81	8.65	6.7	5.34

-log2(p-value)

Figure S6

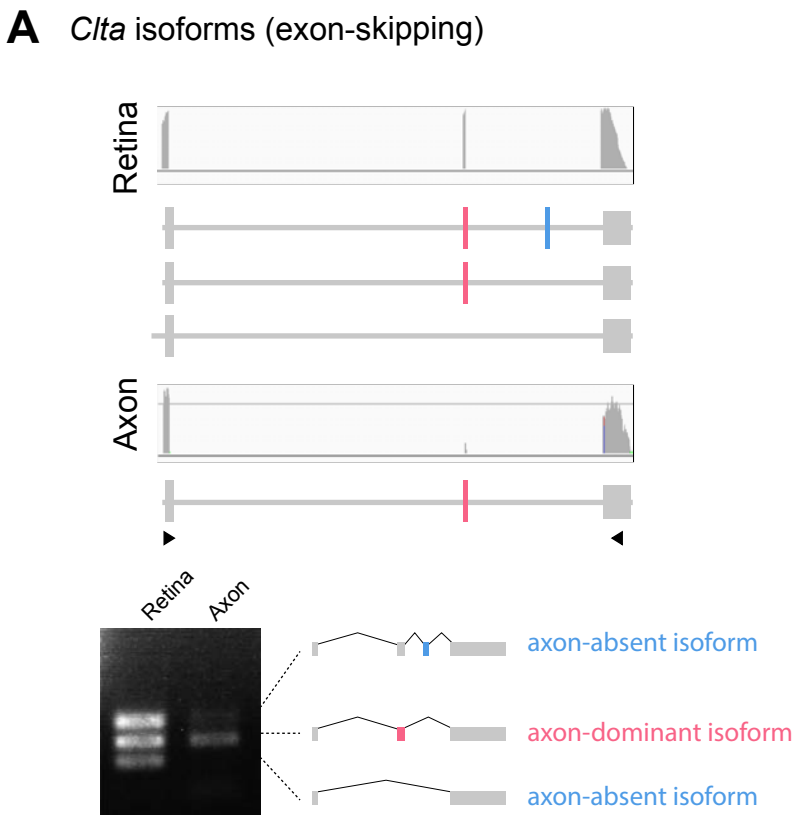

Figure S7